Received: 16 July 2020 | Revised: 8 September 2020 | Accepted: 12 September 2020

DOI: 10.1002/ar.24550

SPECIAL ISSUE ARTICLE

The Anatomical Record | WILEY

A 3D ontogenetic atlas of *Alligator mississippiensis* cranial nerves and their significance for comparative neurology of reptiles

Emily J. Lessner | **Casey M. Holliday**

Program in Integrative Anatomy, Department of Pathology and Anatomical Sciences, University of Missouri School of Medicine, Columbia, Missouri

Correspondence
Emily J. Lessner Program in Integrative Anatomy, Department of Pathology and Anatomical Sciences, University of Missouri School of Medicine, Columbia, MO 65212.
Email: ejlessner@mail.missouri.edu

Funding information
Missouri Research Board; National Science Foundation Division of Earth Sciences, Grant/Award Number: NSF EAR 1631684; University of Missouri Life Sciences Fellowship Program

Abstract

Cranial nerves are key features of the nervous system and vertebrate body plan. However, little is known about the anatomical relationships and ontogeny of cranial nerves in crocodylians and other reptiles, hampering understanding of adaptations, evolution, and development of special senses, somatosensation, and motor control of cranial organs. Here we share three dimensional (3D) models an of the cranial nerves and cranial nerve targets of embryonic, juvenile, and adult American Alligators (*Alligator mississippiensis*) derived from iodine-contrast CT imaging, for the first time, exploring anatomical patterns of cranial nerves across ontogeny. These data reveal the tradeoffs of using contrast-enhanced CT data as well as patterns in growth and development of the alligator cranial nervous system. Though contrast-enhanced CT scanning allows for reconstruction of numerous tissue types in a nondestructive manner, it is still limited by size and resolution. The position of alligator cranial nerves varies little with respect to other cranial structures yet grow at different rates as the skull elongates. These data constrain timing of trigeminal and sympathetic ganglion fusion and reveal morphometric differences in nerve size and path during growth. As demonstrated by these data, alligator cranial nerve morphology is useful in understanding patterns of neurological diversity and distribution, evolution of sensory and muscular innervation, and developmental homology of cranial regions, which in turn, lead to inferences of physiology and behavior.

KEYWORDS

alligator, contrast-enhanced CT, cranial muscles, embryo, homology

1 | INTRODUCTION

The American alligator (*Alligator mississippiensis*) has long been the subject of numerous anatomical studies focusing on all aspects of form and function (e.g., Allen, Elsey, Jones, Wright, & Hutchinson, 2010; Busbey III, 1989; Dufeau & Witmer, 2015; Erickson, Lappin, & Vliet, 2003; Ferguson, 1984; Holliday, Tsai, Skiljan, George, & Pathan, 2013; Rieppel, 1993; Wedin, 1953) and as an accessible member of the pseudosuchian line, has also been used as an evolutionary model for the extant crocodylian condition (e.g., Colbert, Cowl es, & Bogert, 1946; George & Holliday, 2013; Gign ac & Erickson, 2016; Müller & Alberch, 1990; Tsai &

This article includes AR WOW Videos. Video 1 can be viewed at https://players.brightcove.net/656326989001/default_default/index.html?videoId=6206403048001

Holliday, 2011). Alligators and other crocodilians experience marked changes in the shape of the skull, sensory capsules, cranial musculature, and other cranial organ systems during development from dorsoventrally tall-skulled hatchings to flat-skulled adults (e.g., Dodson, 1975; Dufeau & Witmer, 2015; Fabbri et al., 2017; Monteiro, Cavalcanti, & Sommer III, 1997; Sellers, Middleton, Davis, & Holliday, 2017; Tsai & Holliday, 2011). Yet we know little about how the cranial nerves accompany these ontogenetic changes in passage to and from cranial organs. Crocodilian cranial nerve morphology, has been described previously (e.g., Bellairs & Shute, 1953; Lakjer, 1926; Poglayen-Neuwall, 1953; Reese, 1915; Schumacher, 1973; Shaker & El-Bably, 2015; Shiino, 1914) but illustrations have been limited to two-dimensional projections usually following dissection. New contrast-enhanced imaging approaches offer holistic views of the peripheral cranial nervous system and reveal morphological changes during ontogeny.

Here we provide a three-dimensional anatomical atlas of *Alligator mississippiensis* cranial nerves to better describe their relative positions, topology, and targets and show how these change through ontogeny. Using these new data, we discuss the tradeoffs of the method and caution against using contrast-enhanced CT data without supplementary dissection or histological comparison. These new morphological data from cranial nerves are critical to resolving questions in crocodilian biology and vertebrate evolution including: what patterns of neurological diversity exist in crocodilians, archosaurs, and tetrapods; when the acquisition of extreme somatosensation occurred in the pseudosuchian and avian lineages and whether similar acquisition occurred in other lineages (Cunningham, Castro, & Alley, 2007; George & Holliday, 2013; Leitch & Catania, 2012; Soares, 2002); what patterns of neurological distribution to cranial dermatomes exist in crocodilians, archosaurs, and tetrapods (Hieronymus & Witmer, 2010; Holliday & Witmer, 2007); and what is the developmental biology of various skull regions (Holliday & Witmer, 2007, 2009; Klembara, 2001). Finally, we offer an accompanying library of 3D interactive models of the head and cranial nerves of *Alligator* for use in research and public education.

2 | MATERIALS AND METHODS

This project features four *Alligator mississippiensis* specimens from Rockefeller State Refuge, Grand Chenier, Louisiana. The first is an adult specimen with a skull length of 25.4 cm (MUVC AL606). The removed head was fixed in 10% neutral buffered formalin and immersed in 12.3% I_2KI (Lugol Solution, Carolina Biological Supply Company, NC) for 3 years and 7 months. The scan for this specimen was conducted on a NSI scanner using 220 kV, 0.14 mA, and a voxel size of 87.5 μm.

The second is a 12-month-old specimen (MUVC AL031; also used in Holliday et al., 2013; Sellers et al., 2017; Lessner et al., 2019) with a skull length of 5.7 cm. The removed head was fixed in 10% neutral buffered formalin, stored in 70% ethanol, and immersed in 12.3% (w/v) I_2KI (Lugol Solution, Carolina Biological Supply Company, NC) for 5 weeks. The scan for this specimen was conducted on a Zeiss Xradia Versa 510 using 120 kV, 0.083 mA, and a voxel size of 39.42 μm.

The third is an embryonic, stage 19, 27–28 day specimen (MUVC AL089) (Ferguson, 1985) with a head length of 1.4 cm. The entire embryo was fixed in 10% neutral buffered formalin and stabilized using the modified STABILITY protocol (Wong, Spring, & Henkelman, 2013) of Carlisle and Weisbecker (2016). The specimen was then stained overnight in 1% (w/v) I_2KI (Lugol Solution, Carolina Biological Supply Company, NC) and embedded in 1% agarose gel for stabilization during CT scanning. The scan for this specimen was conducted on a Zeiss Xradia Versa 510 using 80 kV and a voxel size of 20.723 μm.

The fourth is a specimen with a 9.8 cm skull length (MUVC AL623). The removed head was bisected, fixed in 10% neutral buffered formalin, and scanned with a voxel size of 51.92 μm on a Siemens Inveon MicroCT scanner at the University of Missouri Biomolecular Imaging Center.

Scan data were imported as DICOM files into Avizo v.9 for segmentation. Structures of interest (see Table 1 and Figure 1) were segmented manually using thresholding and the magic wand and paintbrush tools.

3 | RESULTS

3.1 | Specimen suitability

Of the three contrast-enhanced and scanned specimens, MUVC AL031 provided the most data. The specimen was fully stained (partially overstained, specifically in the middle-ear region) allowing for contrast between muscles, nerves, bone, cartilage, and some vasculature. The embryonic specimen (MUVC AL089) was scanned at a higher resolution than the others because of its small size but it was unclear whether stain had not bound to finer nerve branches, higher resolution is required, or these branches have not yet formed. The STABILITY protocol discussed above and embedding in 1% agarose noticeably enhanced the scan (e.g., eliminated shrinkage, increased staining) in comparison to a previously stained and scanned embryo that was not subjected to this protocol.

TABLE 1 Anatomical abbreviations and structure locations by figure

Abbreviations	Structure	Figure
CN I	Cranial nerve 1 (*N. olfactorius*)	3,4A,6,8,9(A)
CN II	Cranial nerve 2 (*N. opticus*)	3,4B,5(A,D),6,8,9(A)
CN III	Cranial nerve 3 (*N. oculomotorius*)	3,4B,5(A,D),6,8,9(A)
mOv	Inferior oblique muscle (*M. obliquus ventralis*)	5
mRd	Superior rectus muscle (*M. rectus dorsali*)	5
mRm	Medial rectus muscle (*M. rectus medialis*)	4B,5
nRv	Inferior rectus muscle (*M. rectus ventralis*)	4B,5
nOv	Branch to inferior oblique muscle (*N. obliquus ventralis*)	3
nRd	Branch to superior rectus muscle (*N. rectus dorsalis*)	3
nRm	Branch to medial rectus muscle (*N. rectus medialis*)	3
CN IV	Cranial nerve 4 (*N. trochlearis*)	3,4,5(A,D),6,8,9(A)
mOd	Superior oblique muscle (*M. obliquus dorsalis*)	5
CNV	Cranial nerve 5 (*N. trigeminus*)	4B,5(A,D),6,8,9(A),10,11(A,D),14
mAMEM	Adductor mandibulae externus medialis	11
mAMEP	Adductor mandibulae externus profundus	11
mAMES	Adductor mandibulae externus superficialis	11
mAMP	Adductor mandibulae posterior	11
mCN	Constrictor nares	10
mDN	Dilator nares	10
mIRA	Intramandibularis	11
mLB	Levator bulbi	4B,5,11
mPSTp	Pseudotemporalis profundus	11
mPSTs	Pseudotemporalis superficialis	11
mPTd	Pterygoideus dorsalis	11
mPTv	Pterygoideus ventralis	11
nA	Branch to alveoli (*R. alveolares*)	10
nAi	Inferior alveolar branch	10
nAMEM	Branch to adductor mandibulae externus medialis	11
nAMEP	Branch to adductor mandibulae externus profundus	11
nAMP	Branch to adductor mandibulae posterior	11
nAO	Angulus oris	10B,11
nAs	Superior alveolar branch	10
nCA	Ramus caudalis	11
nCU	Cutaneous branch (*R. cutanei*)	10,11C
nGV	Gingival branch	10
nIMA	Branch to intermandibularis	10B,11
nIO	Oral intermandibular branch	10B
nIRA	Branch to intramandibularis	10B,11
nJU	Jugal branch	10B,11
nLG	Lingual branch (*R. lingualis*)	10

(Continues)

TABLE 1 (Continued)

Abbreviations	Structure	Figure
nM	Mucosal branch	10B
nMa	Middle intermandibular branch (*R. mylohyoideus anterior*)	10B
nMK	Meckelian branch	10B
nMp	Caudal intermandibular branch (*R. mylohyoideus posterior*)	10,11
nN	Branch to narial musculature	10B
nNl	Lateral nasal branch (*R. lateralis nasi*)	10
nNm	Medial nasal branch (*R. medialis nasi*)	10
nPAL	Palatine branch	10
nPSTs	Branch to pseudotemporalis superficialis	11
nPT	Branch to pterygoideus muscles (*R. pterygoideus*)	11
nPTd	Branch to pterygoideus dorsalis	10,11
nPTv	Branch to pterygoideus ventralis	10B,11
nRC	Recurrent cutaneous branch	10B
nSO	Supraorbital branch (*N. supraorbitalis*)	10,11
nTYM	Tympanic branch	10,11
V_1	Ophthalmic division (*N. ophthalmicus*)	4B,5,10,11,14
V_2	Maxillary division (*N. maxillaris*)	4B,5,10,11,14
V_3	Mandibular division (*N. mandibularis*)	4,5,10,11,14
V_g	Trigeminal ganglion (*Ganglion trigeminale*)	10,11,14A
V_{g1}	Ophthalmic ganglion (*Ganglion profundal*)	6,10C,11D,14B
$V_{g2/3}$	Maxillomandibular ganglion (*Ganglion gasserian*)	6,10C,11D,14B
CN VI	Cranial nerve 6 (*N. abducens*)	3,4C,5(A,D),8,9(A)
mRl	Lateral rectus muscle (*M. rectus lateralis*)	5
CNVII	Cranial nerve 7 (*N. facialis*)	4C,6,8,9(A),12,13(A,E),14
VII_g	Geniculate ganglion (*Ganglion geniculi*)	12,13,14
mCCa	Constrictor colli pars anterior	13
mCCp	Constrictor colli profundus	13
mDA	Depressor auriculae	13
mDM	Depressor mandibulae	13
mDP	Depressor palpebrae	13
mIMA	Intermandibularis	13
mLA	Levator auriculae	13
mLP	Levator palpebrae	13
nCC	Branch to constrictor muscles	12C
nCHT	Chorda tympani	14
nDM	Branch to depressor mandibulae	12C
nHYM	Hyomandibular division (*N. hyomandibularis*)	6,12,14
nPAL	Palatine division (*N. palatinus*)	12,14
CN VIII	Cranial nerve 8 (*N. vestibulocochlearis*)	6,8,9(A),12
nC	Cochlear branch (*N. cochlearis*)	12
nAc	Branch to caudal ampulla (*N. ampullaris caudalis*)	12

TABLE 1 (Continued)

	Abbreviations	Structure	Figure
	nAl	Branch to lateral ampulla (*N. ampullaris lateralis*)	12
	nAr	Branch to rostral ampulla (*N. ampullaris rostralis*)	12
	nV	Vestibular branch (*pars vestibularis/ampullaris*)	12
	CN IX	Cranial nerve 9 (*N. glossopharyngeus*)	4,6,8,9(A),12,15(A,C)
	IX_g	Petrosal ganglion	4D,9,12
	mBHd	Branchiohyoideus dorsalis	15
	mBHv	Branchiohyoideus ventralis	15
	nTYM	Tympanic branch	12B
	CN X	Cranial nerve 10 (*N. vagus*)	4,6,8,9(A),12,16(A)
	mCL	Laryngeal constrictors (*Constrictor larynges*)	16
	mCR	Cricoarytenoid (*Cricoarytenoideus*)	16
	nPHL	Pharyngolaryngeal branch	12
	nTYM	Tympanic branch	12
	nX	Vagal branch	12
	X_g	Vagus ganglion	4D,12
	CNXII	Cranial nerve 12 (*N. hypoglossus*)	4,6,8,9(A),12,17(A,D)
	mEB	Episternobranchialis	17
	mEBT	Episternobranchiotendineus	17
	mGG	Genioglossus	17
	mGH	Geniohyoideus	17
	mHG	Hyoglossus	17
	mT	Intrinsic muscles of the tongue	17
	nCV	Cervical branch (*R. cervicalis*)	12B
	OTHER		
	aCO	Carotid artery	7C
	cCQ	Cranioquadrate canal	7C
	C_g	Ciliary ganglion	6
	CT	Cartilago transiliens	11A
	dBS	Basisphenoid diverticulum	7D
	dITY	Intertympanic diverticulum	7D
	dPA	Parietal diverticulum	7D
	dPT	Pterygoid diverticulum	7D
	f	Foramen	7
	fL	Lymphatic foramen	7D
	fMAG	Foramen magnum	7
	fPS	Foramen from basisphenoid diverticulum to pharyngotympanic sinus	7D
	nSYM	Sympathetic nerve	6
	P_g	Palatine ganglion	6
	S_g	Sympathetic ganglion	6,9
	vJG	Jugular vein	7C

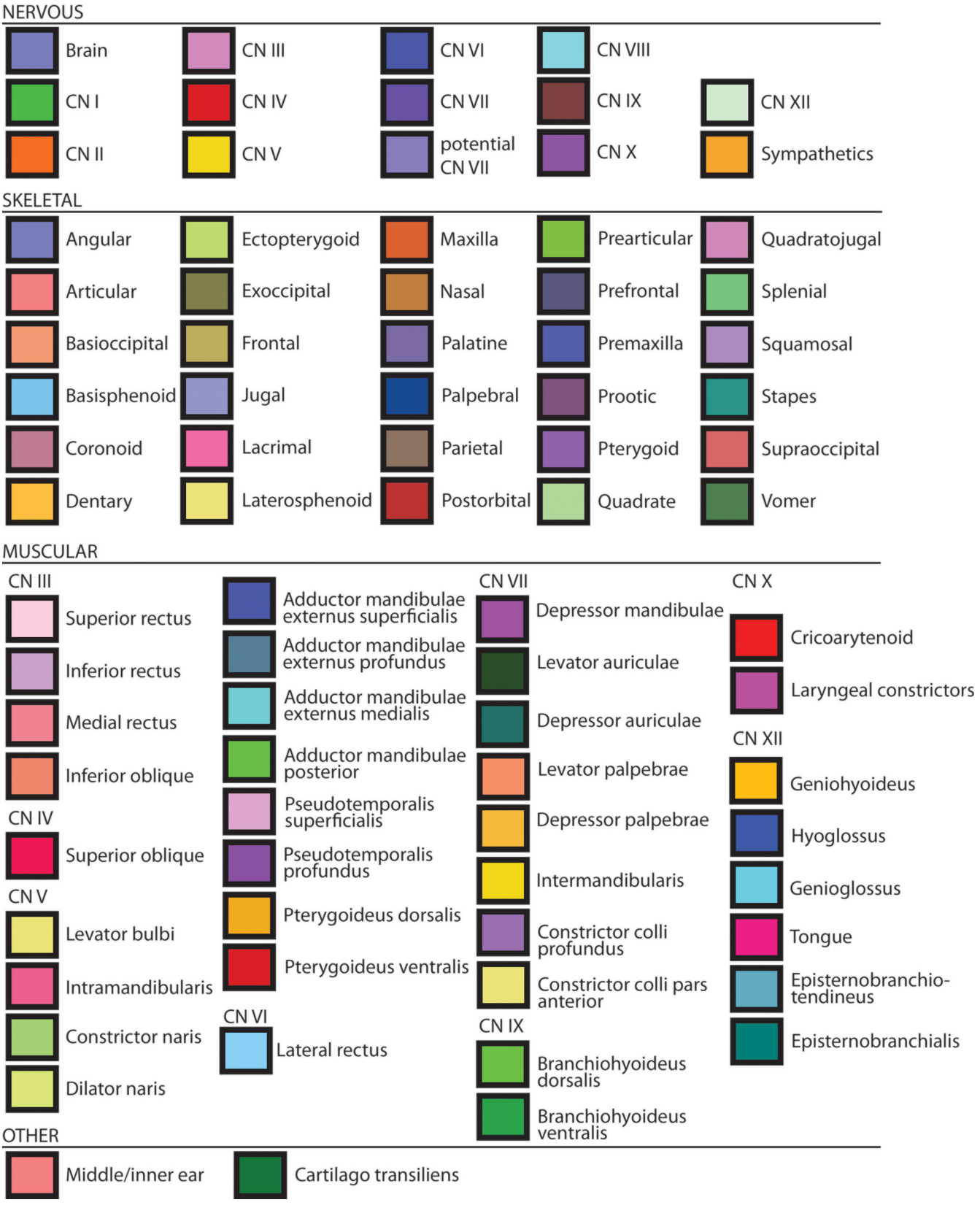

FIGURE 1 Color guide to segmented structures

The largest specimen (MUVC AL606), even after years of staining, exhibited lower contrast between structures either because of incomplete stain penetration and binding to the deepest structures or limited x-ray penetration.

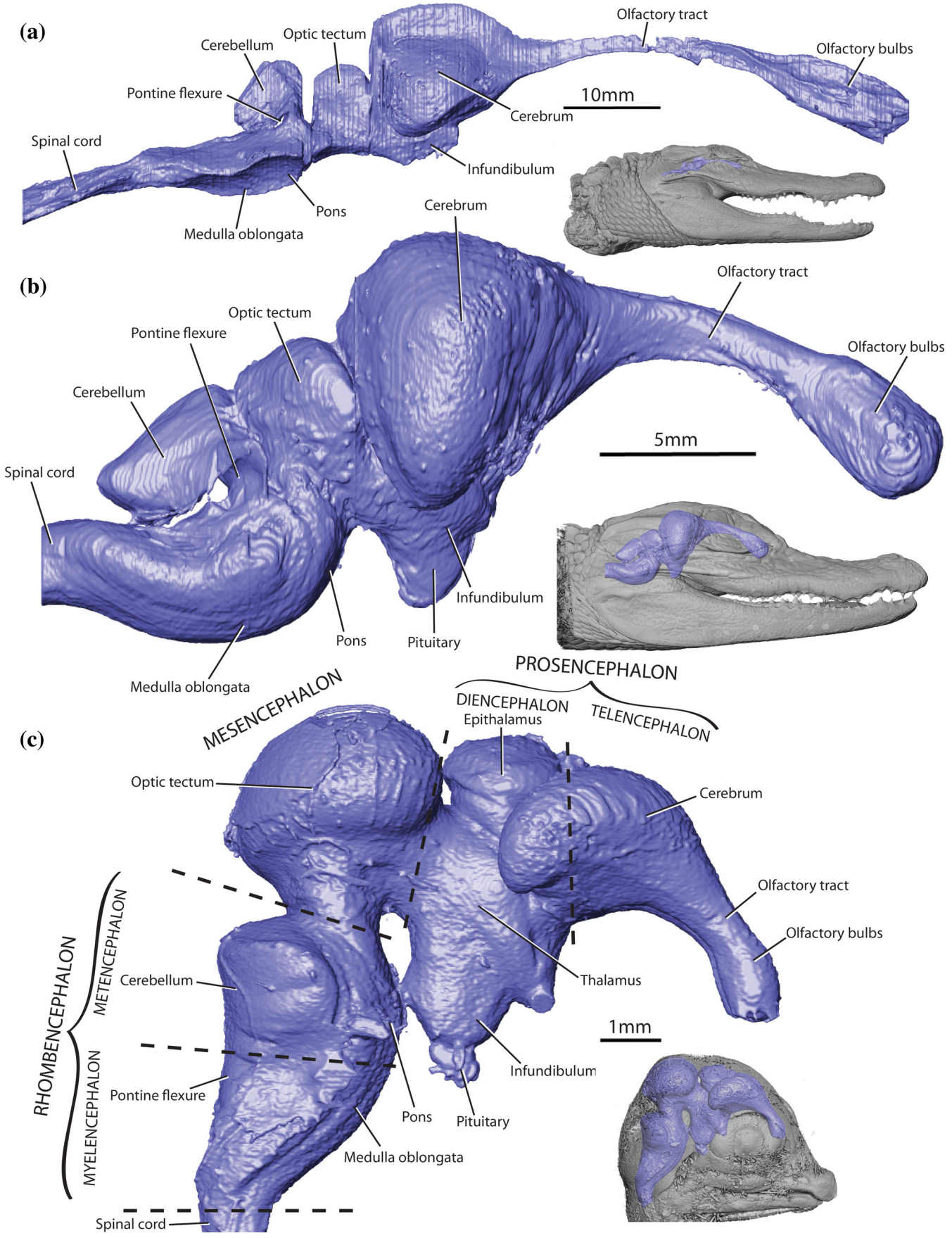

FIGURE 2 Brain. 3D reconstruction of the brain, brain regions, and head of alligator MUVC AL606 (a), yearling alligator MUVC AL031 (b), and stage 19 embryo MUVC AL089 (c, mirrored) in right lateral view

Because it was scanned as a whole, its size also limited the minimum resolution of the resulting data. Generally, in the embryo, because the brain has not yet elongated to the adult morphology, nor have the muscles and bones fully formed, the relationships between the nerves and other structures are less clear. Conversely, in the large specimen, because scan resolution is limited by stain penetration and specimen size, relationships between tissues are less clear.

3.2 | Cranial nerve I: Olfactory

The olfactory nerve (CN I) transmits purely sensory signals from air-borne stimuli from olfactory sensory neurons in the nasal cavity to the olfactory bulbs via unmyelinated fibers (Crosby, 1917; Hansen, 2007). The neurons comprising the first cranial nerve are visible as a series of short ventral extensions of the rostral end of the olfactory bulbs (Figures 2 and 3). From the olfactory bulbs, these bundles extend rostroventrally to contact the olfactory epithelium of the nasal cavity (Figure 4). There are no visible ontogenetic differences in the olfactory nerve.

3.3 | Cranial nerve II: Optic

The optic nerve (CN II) transmits purely visual sensory signals. The optic nerve is a short, thick nerve extending from the midline of the telencephalon (Figures 2 and 3). Shortly after its origin from the brain, it passes through the optic chiasm in close contact with the opposing optic nerve. The optic nerve then extends by the rostroventral border of the laterosphenoid. From there it passes dorsal to the *m. rectus ventralis* (mRv, m. inferior rectus), medial to the *m. rectus dorsalis* (mRd, m. superior rectus), and bends ventrally around the *m. levator bulbi* (mLB) to enter the caudomedial aspect of the eye (Figure 5). During ontogeny, the optic nerve elongates rostrocaudally in response to the lengthening of the skull and the more rostral position of the orbits (i.e., with respect to the origin of the nerve from the telencephalon) in the adult.

3.4 | Cranial nerve III: Oculomotor

The oculomotor nerve (CN III) transmits only motor signals and is a long, nerve emerging from the mesencephalon-pontine junction (Figures 2 and 3). It passes through a notch in the ventral border of the laterosphenoid (fCN III) caudoventral to the optic nerve before extending through the ciliary ganglion (C_g) to its destinations (Romer, 1956) (Figures 6-9). In the embryo and yearling alligators (but not the adult), the oculomotor nerve passes laterally around the diencephalon (Figure 3). The ciliary ganglion (Figure 6) of the oculomotor nerve is located dorsal to *m. levator bulbi* and m. lateral rectus (mRl, *m. rectus lateralis*) and inferior to the ophthalmic division of the trigeminal nerve (V_1) where the oculomotor nerve sends a short branch (superior branch, nRd) to the ventral border of the *m. rectus dorsalis* (Figures 5 and 6). The next branch passes laterally, between the *m. levator bulbi* and m. lateral rectus, though its destination is unknown (potentially carrying parasympathetic neurons). A third branch (inferior branch) innervates the *m. rectus ventralis* at its ventral surface, passing dorsal to the m. lateral rectus and extends two more branches. One of these (nRm) innervates the m. medial rectus (mRm, *m. rectus medialis*) and the other (nOv) passes ventral to the eye before innervating the *m. obliquus ventralis* (mOv, m. inferior oblique) (Figure 5). There are no obvious differences in oculomotor nerve anatomy during ontogeny.

3.5 | Cranial nerve IV: Trochlear

The trochlear nerve (CN IV) transmits only motor signals as well and is a long, thin nerve extending from the dorsolateral surface of the caudal midbrain (Figures 2 and 3). It extends laterally around the brain, ventral to the cerebrum. In the yearling and adult alligator, the nerve passes in close proximity to the ventral cerebrum, whereas in the embryo the cerebrum has not completed growth and therefore the trochlear nerve is well ventral to it. From there, it passes through a foramen in the laterosphenoid (fCN IV) caudal to the optic nerve (Figure 7–9). The trochlear nerve continues rostrally to innervate the *m. obliquus dorsalis* (mOd, m. superior oblique) from a ventral aspect, passing caudal to the *m. rectus dorsalis*, dorsal to the m. medial rectus, superior to the ophthalmic division of the trigeminal nerve, and medial to the eye (Figures 4 and 5). As with the oculomotor nerve, there are no obvious ontogenetic differences in trochlear nerve anatomy.

3.6 | Cranial nerve V: Trigeminal

The path of the *Alligator* trigeminal nerve (CN V) has been covered extensively in the literature (e.g., George & Holliday, 2013; Holliday & Witmer, 2007; Holliday & Witmer, 2009; Iordansky, 1964; Leitch & Catania, 2012; Poglayen-Neuwall, 1953; Schumacher, 1973) and so will be summarized here. The trigeminal nerve transmits both

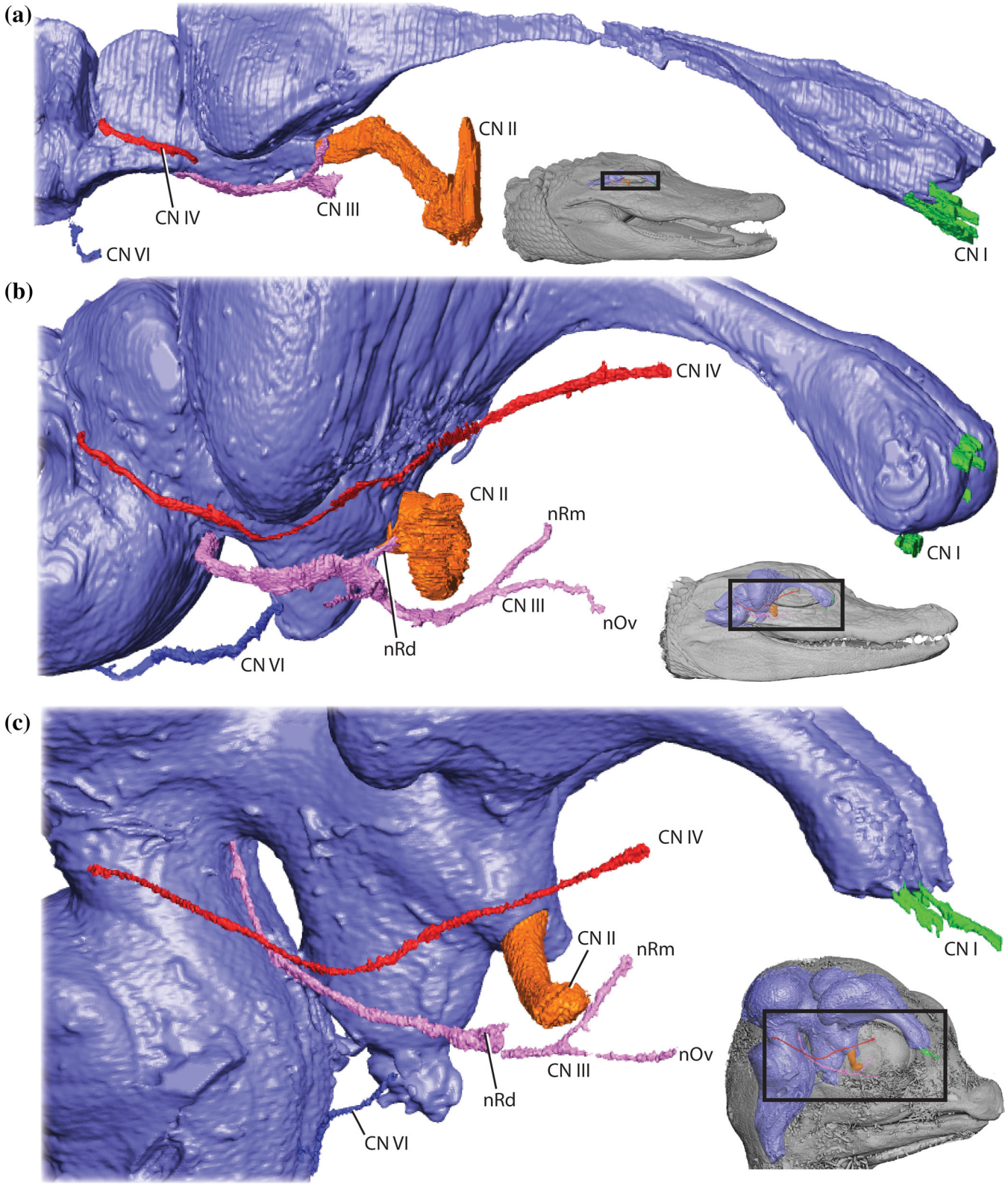

FIGURE 3 Olfactory, Optic, Oculomotor, Abducens, and Trochlear Nerves. 3D reconstruction of the brain, cranial nerves I to VI (excluding V), and head of alligator MUVC AL606 (a), yearling alligator MUVC AL031 (b), and stage 19 embryo MUVC AL089 (c, mirrored) in right rostrolateral view

motor and sensory signals, beginning at the pons, and extending roots to the trigeminal ganglion (V_g) through a large foramen (fCN V) bounded by the prootic and laterosphenoid (Figures 2, 7, and 10). The trigeminal

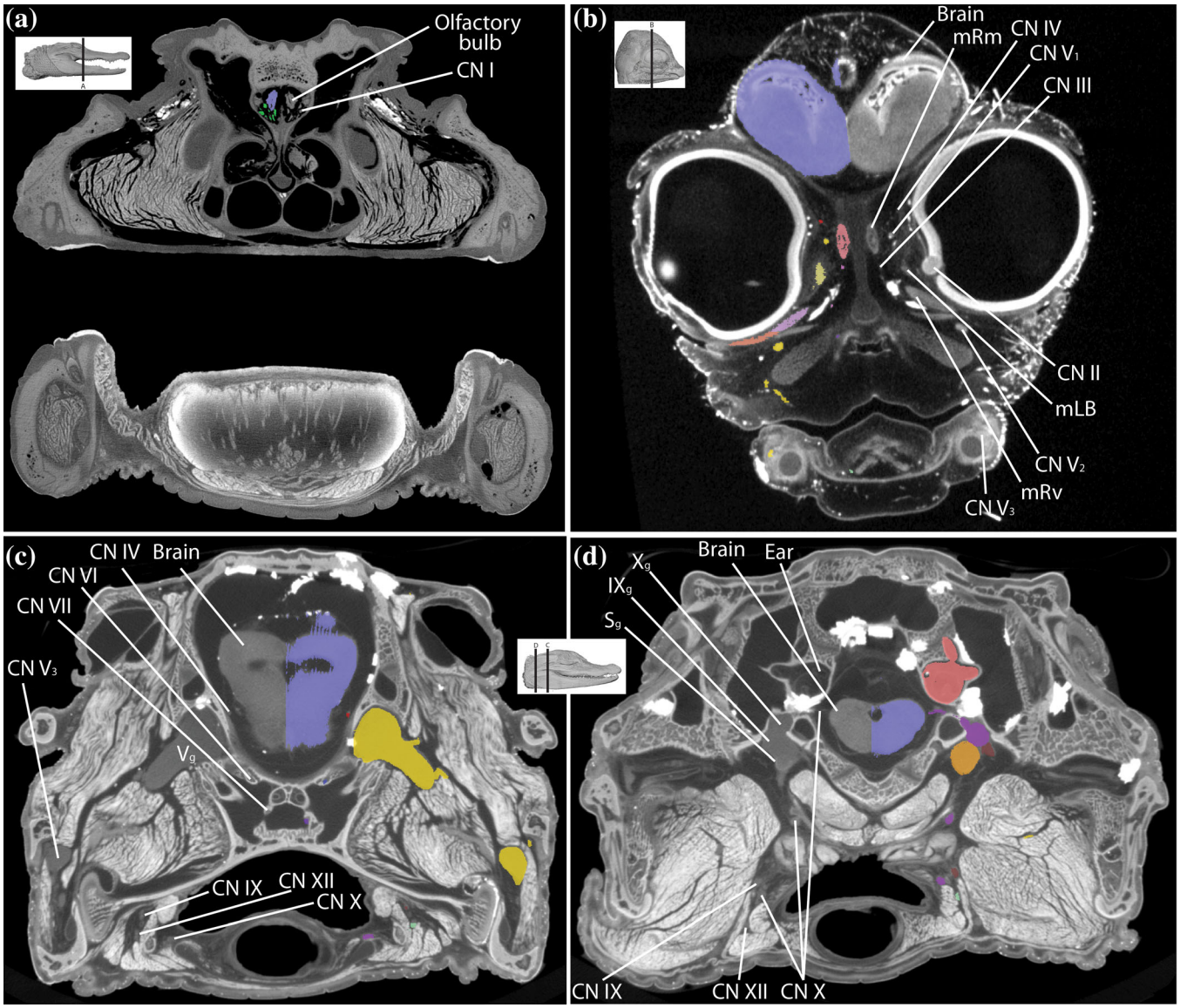

FIGURE 4 Cross Sectional Data. Axial slices through segmented CT data of alligator MUVC AL606 (a), stage 19 embryo MUVC AL089 (b), and yearling alligator MUVC AL031 (c, d)

ganglion sits within the trigeminal fossa, formed by the prootic, laterosphenoid, quadrate and pterygoid (Figures 7–9) and comprises two smaller ganglia. The maxillomandibular ganglion ($V_{g2/3}$) is larger, and more caudoventral than the smaller, rostrodorsally located ophthalmic ganglion (Figure 10, V_{g1}). Through ontogeny, there is less distinction between the ophthalmic and maxillomandibular ganglia; two distinct ganglia are visible in the embryonic alligator, less so in the yearling, and not at all in the adult alligator. Also, the merged trigeminal ganglion becomes larger relative to brain size as specimen size increases.

The ophthalmic division of the trigeminal nerve (V_1) extends rostrally through a foramen in the laterosphenoid and passes along the ventral surface of the laterosphenoid dorsal to the *m. levator bulbi* and m. lateral rectus and lateral to the oculomotor nerve (Figure 6). Before continuing rostrally, a branch (nFR) extends dorsally from the ophthalmic ganglion, passing caudal to the orbit and extending to the frontal (Figure 10). The ophthalmic nerve continues rostrally, passing through the *m. rectus dorsalis* and dorsal to the optic nerve. From there it courses rostrally, medial to the eye, ventral to the trochlear nerve, dorsal to the m. medial rectus, then ventrolateral to the *m. obliquus dorsalis* before paralleling the olfactory bulbs. The terminal ophthalmic branches, the medial and lateral nasal branches (nNm, nNl), extend rami through various foramina on the surface of the nasals and premaxillae to innervate the integument of the dorsomedial portion of

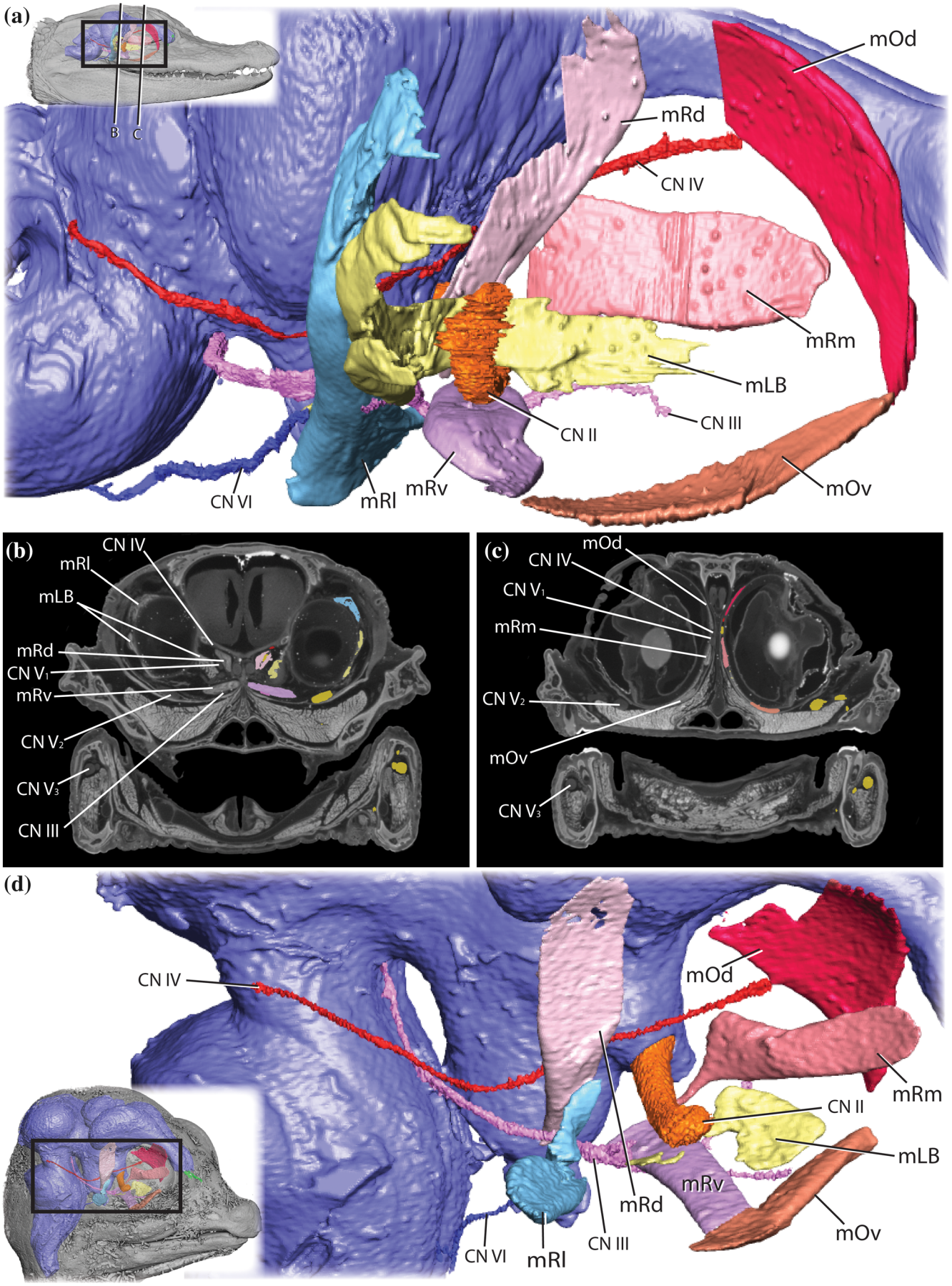

FIGURE 5 Legend on next page.

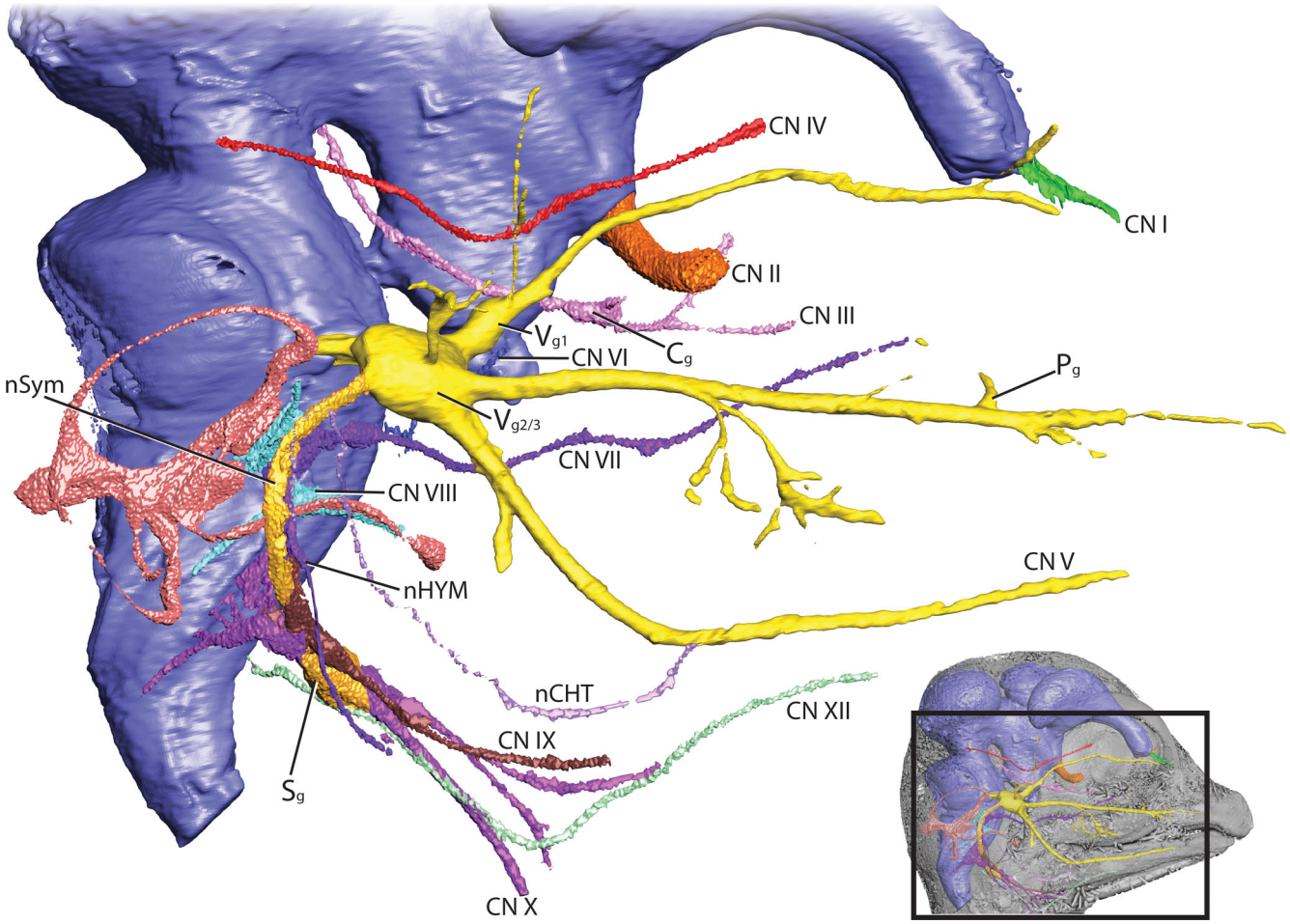

FIGURE 6 Autonomic Nerves. 3D reconstruction of the brain, cranial nerves, autonomic structures, and head of stage 19 embryo MUVC AL089 (mirrored) in right lateral view. A 3D model of the figure may be found at: https://sketchfab.com/3d-models/embryonic-alligator-cranial-nerves-b14a75f97da74cd89e402d118ba38e59

the rostrum. The lateral nasal branch also carries parasympathetic fibers rostrally to the narial musculature (nN).

Two small branches extend dorsally from the trigeminal ganglion, the tympanic branch (nTYM), passing through a foramen in the prootic, and the supraorbital ramus (nSO) of the maxillary division (Figure 10). The maxillary (V_2) and mandibular (V_3) divisions extend laterally from the trigeminal ganglion through the trigeminal (maxillomandibular) foramen, formed by the quadrate, pterygoid, and laterosphenoid (Figure 9). The maxillary division passes rostrally, dorsal to the *m. pterygoideus dorsalis* (mPTd) through the ventrolateral portion of the orbit (Figure 11). Before entering the superior alveolar canal in the maxilla, a branch (nJU) extends laterally, perforating the jugal to innervate integumentary receptors. From there it enters the maxilla as the superior alveolar nerve (nAs) and extends branches through various foramina to terminate in sensory receptors in the integument (nCU), gingiva (nGV), and alveoli (nA). Several palatine branches (nP) descend to innervate the palatal mucosa. The superior alveolar nerve continues into the premaxilla lateral to the nasal mucosa.

FIGURE 5 Eye Muscles. 3D reconstruction of the brain, cranial nerves I to VI (excluding V), extraocular muscles, and head of yearling alligator MUVC AL031 (a) and stage 19 embryo MUVC AL089 (d, mirrored) in right rostrolateral view with axial CT slices of MUVC AL031 (b, c). A 3D model of (a) may be found at: https://sketchfab.com/3d-models/yearling-alligator-extraocular-muscles-832ea36447394124b9fa51fbed6bcd9b and a 3D model of (d) may be found at: https://sketchfab.com/3d-models/embryonic-alligator-extraocular-muscles-03ccd7cc21fd40608d6bb4dbd6e61578

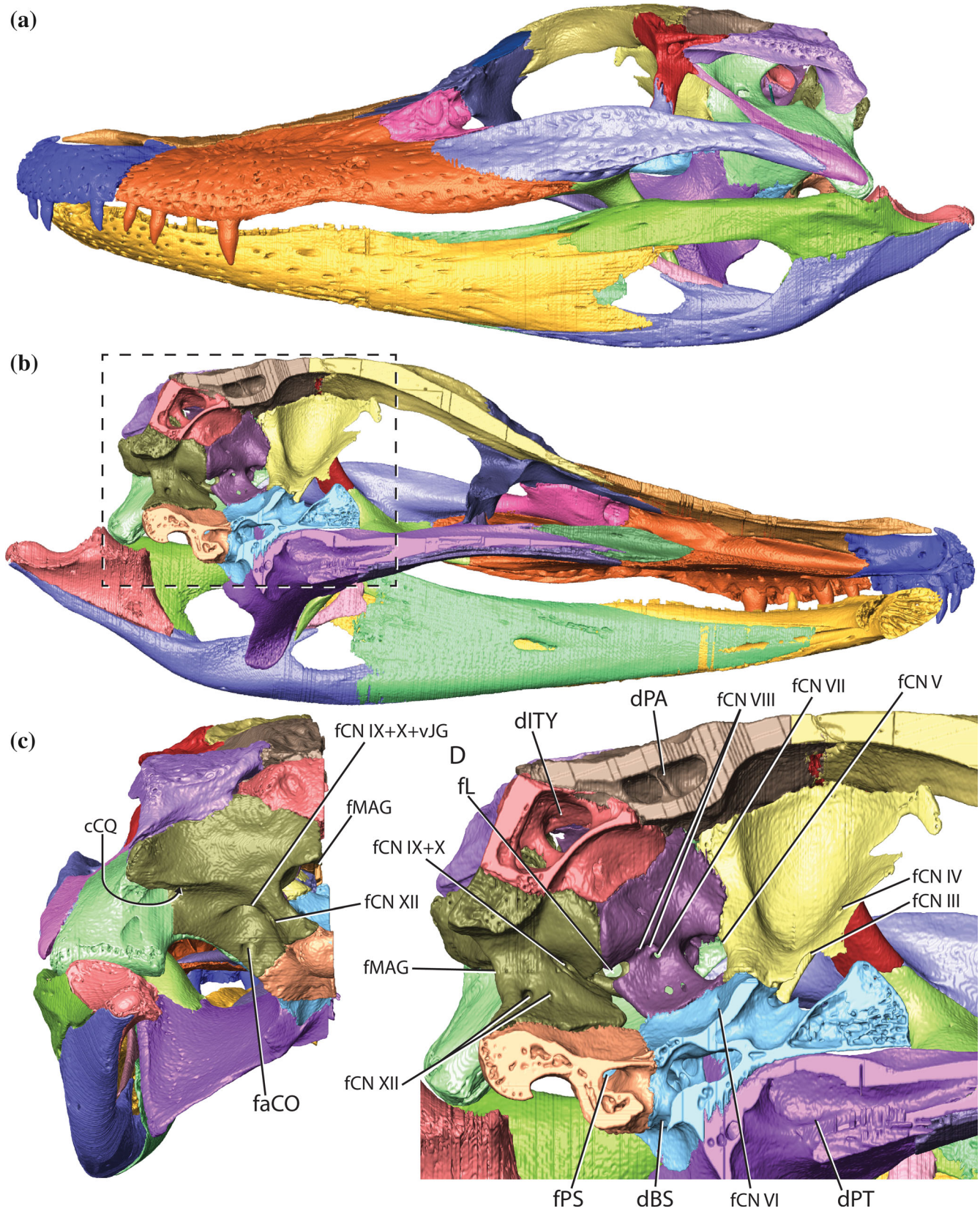

FIGURE 7 Cranial Osteology. 3D reconstruction of alligator (MUVC AL623) cranial elements in left lateral (a), left medial (b), bisected caudal (c), and left medial (d) view. Location of D marked in B. A 3D model of (b) may be found at: https://sketchfab.com/3d-models/alligator-skull-and-cranial-nerves-98c9ca48f3a3408f8c64d6c6d4256aee

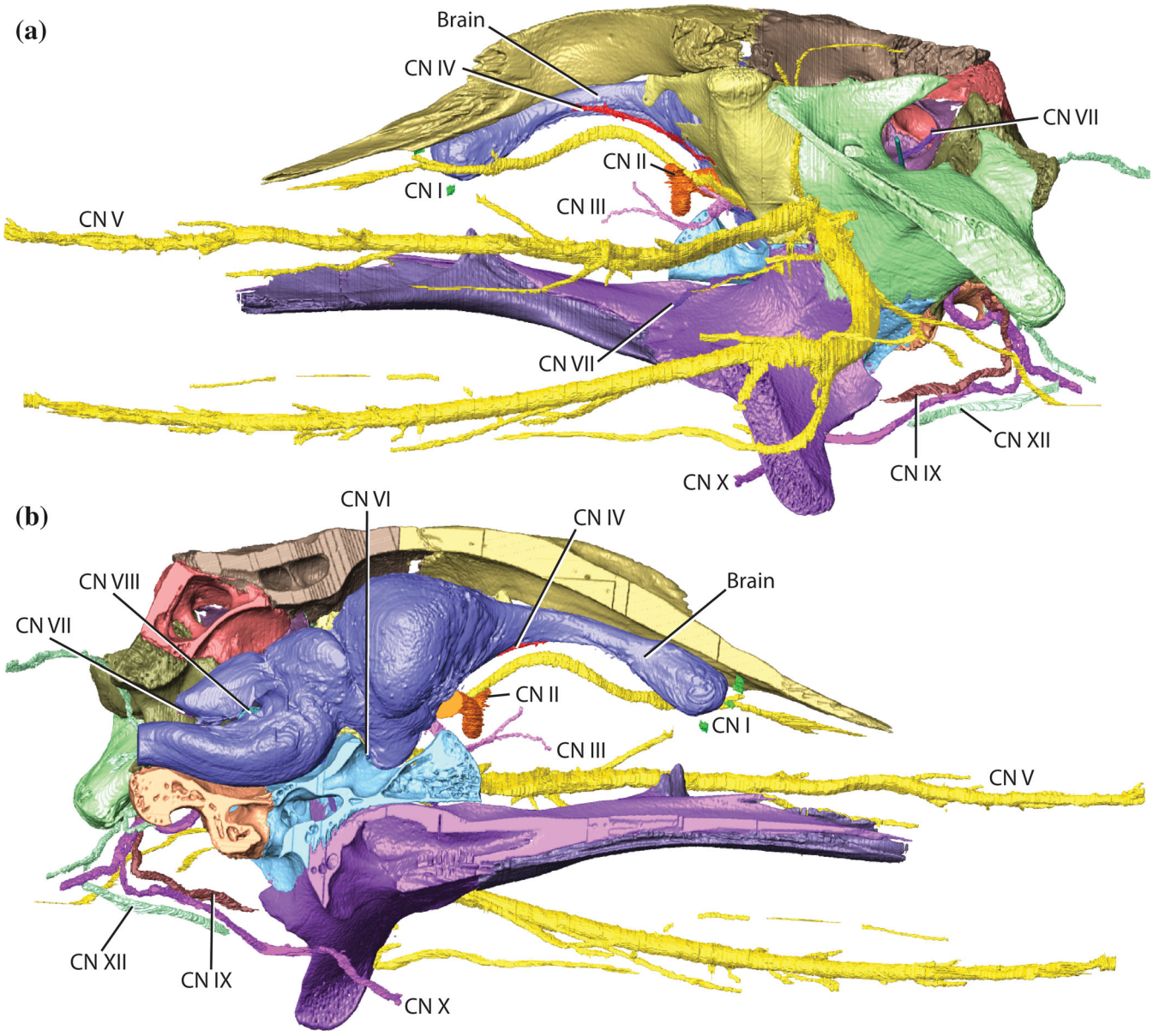

FIGURE 8 Osteological and Nervous Relationships. 3D reconstruction of alligator cranial elements (MUVC AL623), cranial nerves (MUVC AL031), and the brain (MUVC AL031) in left lateral (a) and left medial (b) view. Cranial nerves and brain from MUVC AL031 have been mirrored and transformed to fit the skull of MUVC AL623

The mandibular division extends ventrolaterally after exiting the trigeminal foramen (Figure 11; see the following for detailed descriptions: Poglayen-Neuwall, 1953; Schumacher, 1973; Holliday & Witmer, 2007). Immediately, short branches extend laterally, one (nAMEP) to the *m. adductor mandibulae externus profundus* (mAMEP), followed by two (nAMEM) to the *m. adductor mandibulae externus medialis* (mAMEM). The pterygoid ramus (nPT) extends rostroventrally and divides (extending the nPTd and nPSTs) to innervate the *m. pterygoideyus dorsalis* (mPTd) and the *m. pseudotemporalis superficialis* (mPSTs) (Figure 11). Another branch (nPTv) extends caudoventrally to the *m. pterygoideus ventralis* (mPTv). Further ventrally along the mandibular division, the *ramus caudalis* (nCA) extends laterally and curves rostrally, passing between the *m. adductor mandibulae externus superficialis* (mAMES) and the *m. adductor mandibulae posterior* (mAMP). Another small branch extends caudolaterally to the *m. adductor mandibulae posterior* (nAMP). A sensory branch, the *angulus oris* (nAO), then extends rostrally, receiving sensory input from the caudal border of the oral cavity (Figure 11). From there, the mandibular division loops ventrolaterally bounded by the *m. adductor mandibulae posterior* and the *m. adductor mandibulae internus* medially and the *m. adductor mandibulae externus*

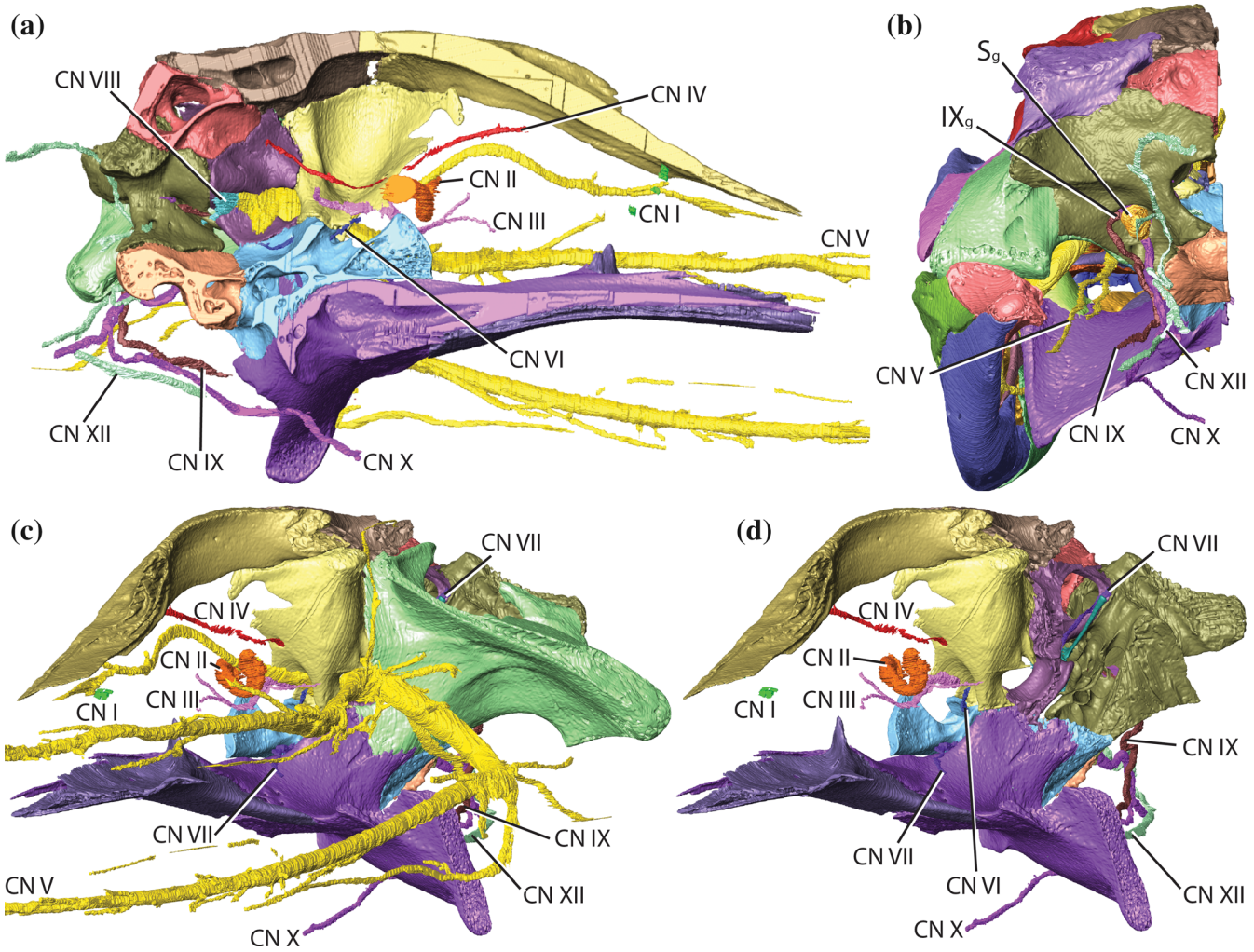

FIGURE 9 Osteological and Nervous Relationships (cont.). 3D reconstruction of alligator cranial elements (MUVC AL623) and nerves (MUVC AL031) in left medial (a), caudal (b), and left rostrolateral (c) views and left rostrolateral view with CNV and the quadrate removed (d). Cranial nerves from MUVC AL031 have been mirrored and translated to fit the skull of MUVC AL623. A 3D model of (a) may be found at: https://sketchfab.com/3d-models/alligator-skull-and-cranial-nerves-98c9ca48f3a3408f8c64d6c6d4256aee

laterally. The recurrent cutaneous branch (nRC) extends caudally just before the rostral extension of the mandibular division. As the mandibular division extends rostrally, a caudal intermandibular branch (nMp) passes ventromedially, extending rami (nIMA) to the *m. intermandibularis* (mIMA) and integument. As the mandibular division passes dorsal to the *m. intramandibularis* (mIRA) and lateral to the *m. intermandibularis*, it extends branches to each (nIMA, nIRA) before entering the inferior alveolar canal (Figure 11). Here a branch to the *m. constrictor colli pars anterior* (mCCa) is expected, but not visible in the data. The middle intermandibular branch (nMa) extends medially, followed by the oral intermandibular branch (nIO), and a branch that travels rostrally with Meckel's cartilage (nMK). Lingual (nLG) and mucosal (nM) rami extend from the oral intermandibular branch. Rostrally, numerous lingual, mucosal, and dental branches (nCU, nA, nM) extend from the inferior alveolar nerve (nAi) to their terminations in the oral cavity, and foramina in the dentary transmit cutaneous branches to their terminations in sensory receptors of the integument of the rostral mandibles (Figure 10).

In the embryonic alligator, the three trigeminal divisions are similar in diameter. However, in the yearling and adult alligator, the ophthalmic division is the smallest and the mandibular division the largest. Additionally, because of the lengthening of the skull and brain, the ventrolateral loop of the mandibular division becomes more defined during ontogeny.

3.7 | Cranial nerve VI: Abducens

The abducens nerve (CN VI) is a short, motor-only nerve, extending from the pontine-medulla junction on the

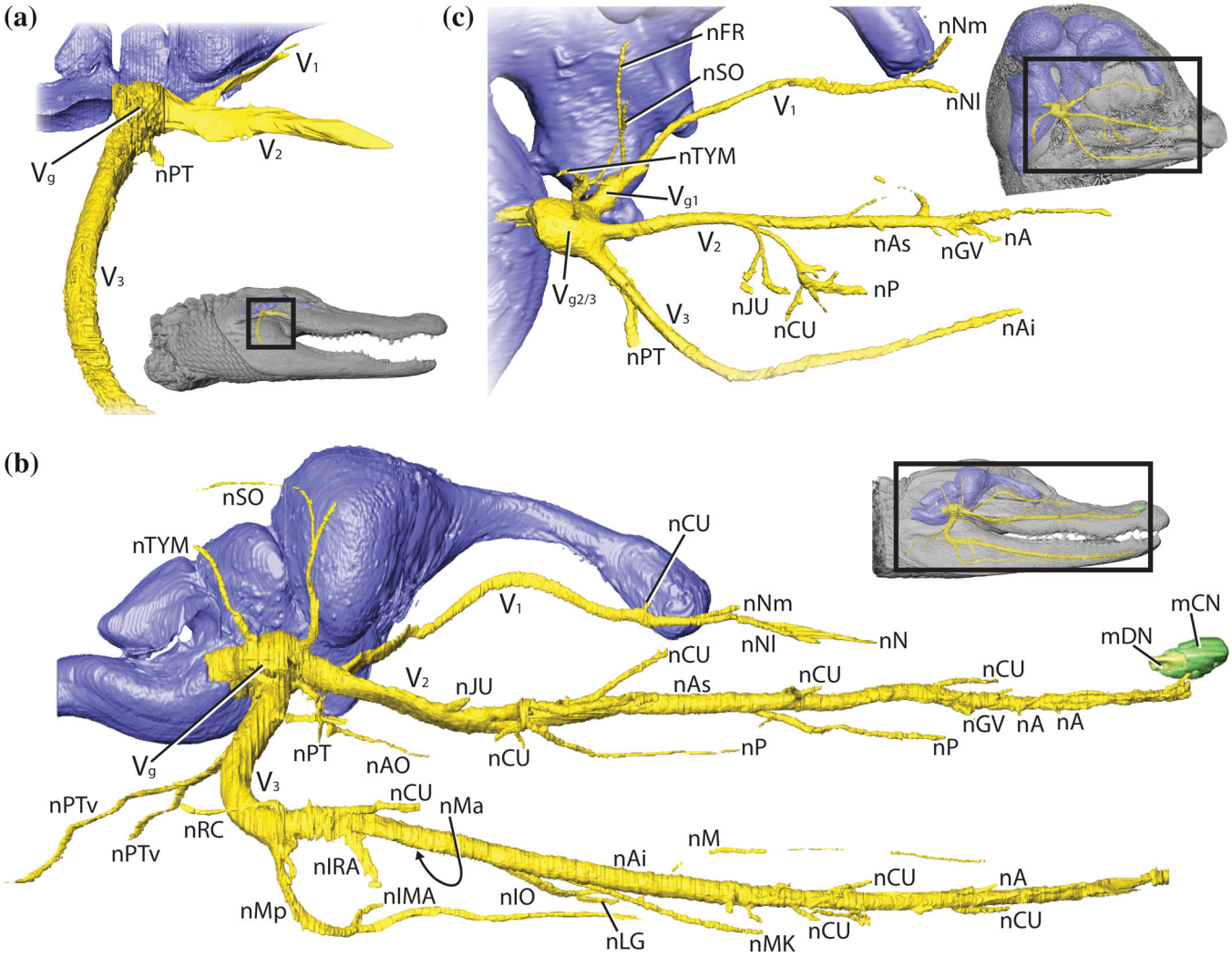

FIGURE 10 Trigeminal Nerve. 3D reconstruction of the brain, cranial nerve V, narial muscles, and head of alligator MUVC AL606 (a), yearling alligator MUVC AL031 (b), and stage 19 embryo MUVC AL089 (C, mirrored) in right lateral view

ventral surface of the brain (Figures 2 and 3). It does so by passing through a canal and foramen (fCN VI) in the basisphenoid lateral to the canal and foramen for the internal carotid artery (Figure 4) (*foramen caroticum anterius* of Iordansky, 1973) (Figures 7 and 9). One third of the extent of the abducens nerve is just dorsal to the endocranial surface of the basisphenoid, a second third within the basisphenoid, and the final third within the orbit approaching the ophthalmic division of the trigeminal nerve and the innervating the m. lateral rectus (Figure 5, mRl). The abducens nerve also innervates the *m. quadratus*, which is responsible for movement of the nictitating membrane of the eye (Stibbe, 1928), but neither this branch nor this muscle are visible in these data. The abducens nerve lengthens rostrocaudally as specimen size increases in response to the lengthening of the skull and brain and the more rostral position (i.e., with respect to the origin of the nerve from the pontine-medulla junction) of the orbits in the adult.

3.8 | Cranial nerve VII: Facial

The facial nerve (CN VII) transmits both motor and sensory signals and extends rostrally and laterally from the pontine-medulla junction through a foramen (fCN VII) in the prootic before immediately passing through the geniculate ganglion (Figures 2 and 12, VII_g). The palatine division (nPAL) extends rostrally and ventromedially from the ganglion where the hyomandibular division (nHYM) extends caudally. The palatine division passes ventrally across the lateral border of the prootic and basipterygoid before extending between the basipterygoid-palatine suture and continuing dorsally along the lateral border of the palatine to the palatine-maxillary suture (Figures 4, 7–9). The hyomandibular division passes dorsolaterally along the lateral border of the prootic to the prootic-opisthotic suture. Here it passes nearby the *m. levator auriculae* (mLA) and *m. depressor auriculae* (mDA) (Figure 13) via a canal to the

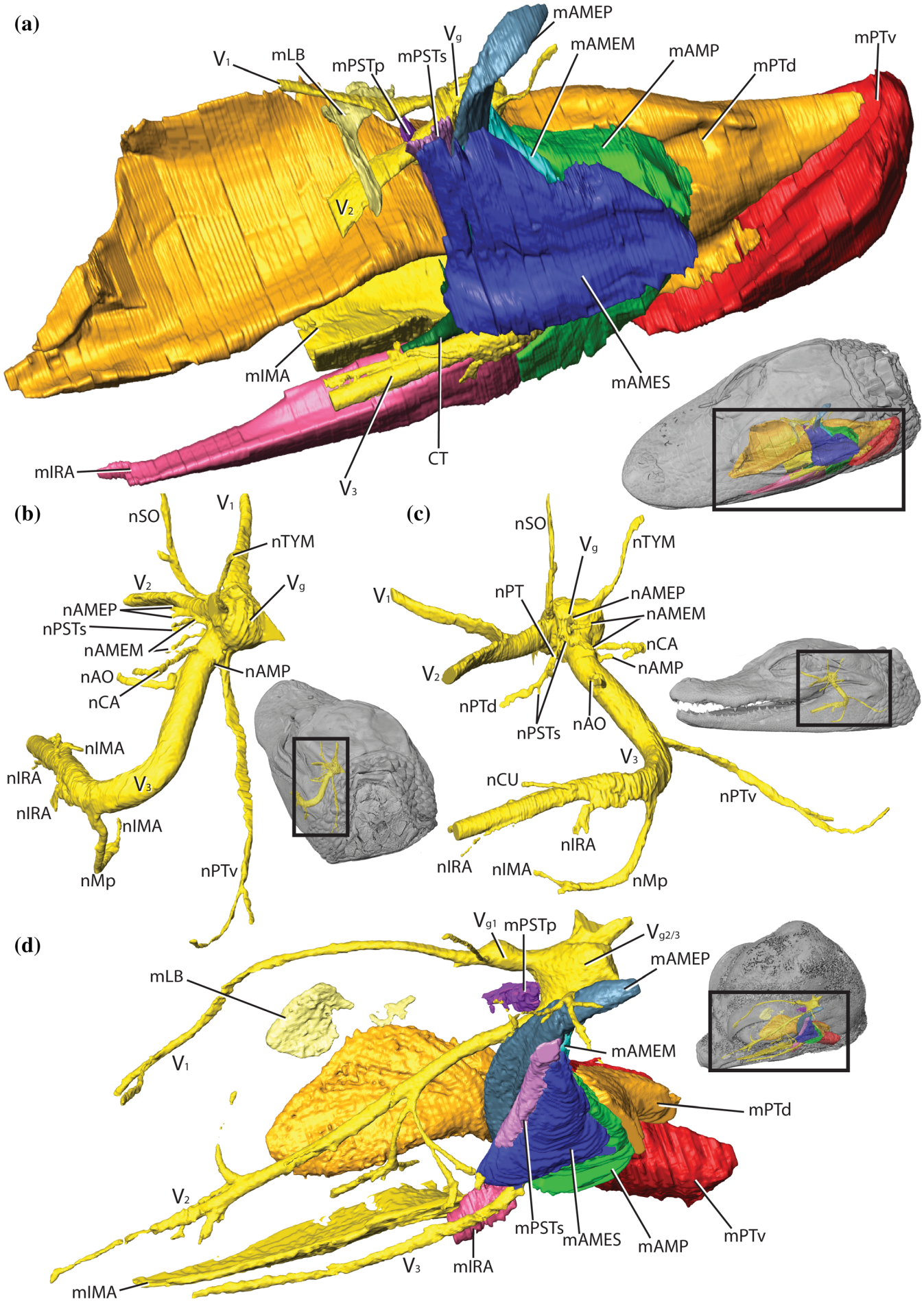

FIGURE 11 Legend on next page.

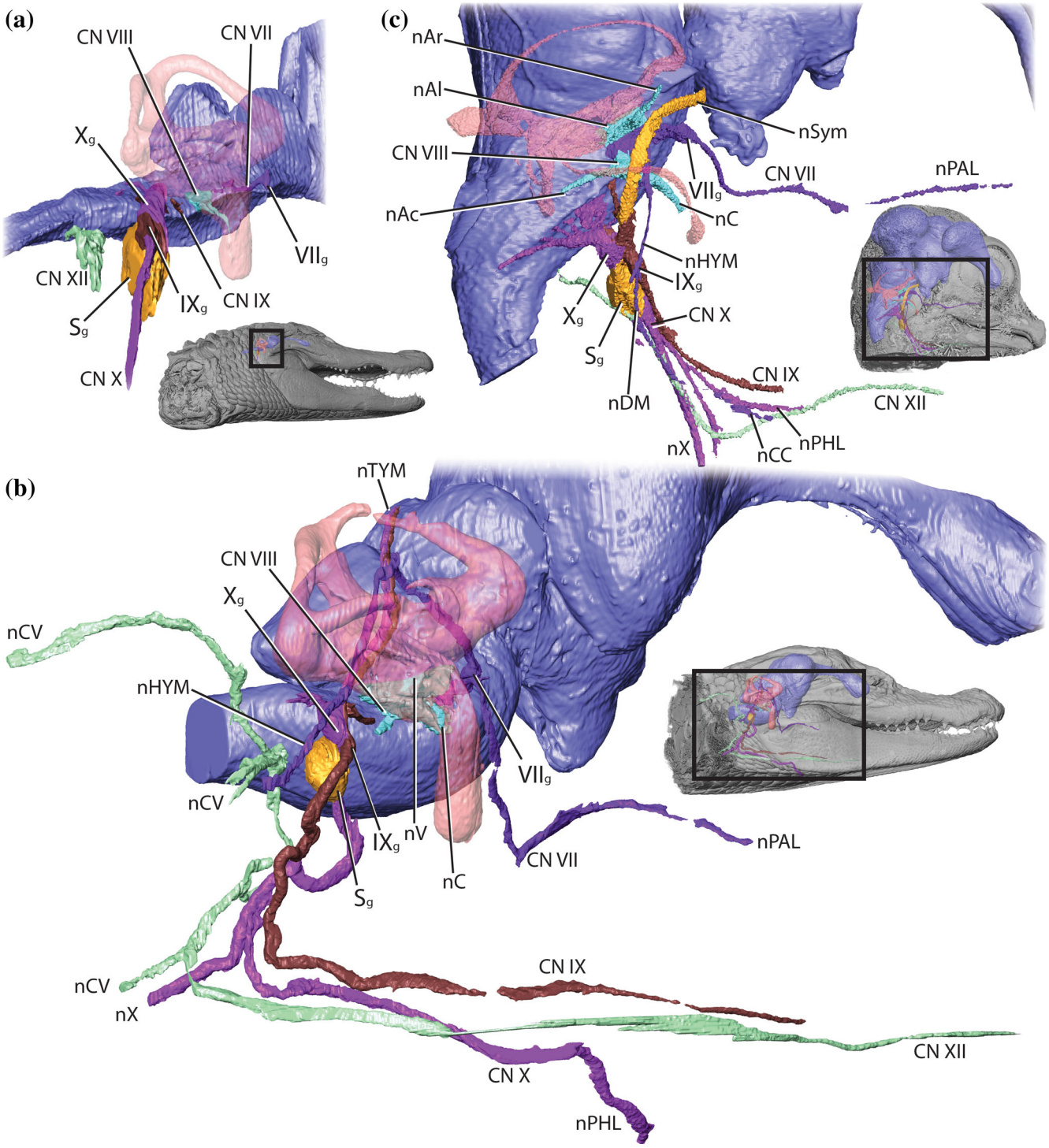

FIGURE 12 Facial, Vestibulocochlear, Glossopharyngeal, Vagus, and Hypoglossal Nerves. 3D reconstruction of the brain, cranial nerves VII to XII (excluding XI), inner and middle ear (transparent), and head of alligator MUVC AL606 (a), yearling alligator MUVC AL031 (b), and stage 19 embryo MUVC AL089 (C, mirrored) in right caudolateral (a, b) and ventrolateral (c) view

FIGURE 11 Trigeminal Nerve-Innervated Muscles. 3D reconstruction of cranial nerve V, the trigeminal nerve-innervated muscles, and head of yearling alligator MUVC AL031 (a) and stage 19 embryo MUVC AL089 (d) in dorsolateral view with muscular branches of MUVC AL031 in left caudolateral (b) and left rostrolateral (c) views. (Colors follow Holliday et al., 2013). A 3D model of (a) may be found at: https://sketchfab.com/3d-models/yearling-alligator-cn-v-innervated-muscles-538568dea57041628e8a5b564b30b2eb and a 3D model of (d) may be found at: https://sketchfab.com/3d-models/embryonic-alligator-cn-v-innervated-muscles-3a7d93f76545415da07e60d46d03c346

paraoccipital process of the exoccipital at the junction of the exoccipital and quadrate (Figure 7, cCQ) (cranioquadrate canal and fissure of Jollie, 1962 and Iordansky, 1973). The hyomandibular division splits into two smaller rami (Bellairs & Shute, 1953; Shiino, 1914), the hyoid ramus of the hyomandibular division (*ramus communicans* of Shiino, 1914) and the chorda tympani (nCHT), but only the beginning of the hyomandibular division and the hyoid ramus are clearly visible in these data, the chorda tympani being too small. The path of the chorda tympani was approximated using the associated vasculature with which it travels (external carotid artery and mandibular vein and artery [Porter, Sedlmayr, & Witmer, 2016]) and the description of Shiino (1914) (Figure 13). The hyomandibular division splits at the level of the foramen magnum and the hyoid ramus extends rami (nDM, nCCp) to innervate the *m. depressor mandibulae* (mDM) and the *m. constrictor colli profundus* (Figures 13 and 14, mCCp). The chorda tympani loops rostrodorsally, ventral to the otic process of the quadrate and dorsomedial to the stapes before continuing ventrally, first lateral to the quadrate and rostral to the stapes along the rostral wall of the tympanic cavity, then medial to the mandibular joint (Shiino, 1914 [see Text-figure 33]; Goodrich, 1915; Hotton, 1960). This loop is followed by a ventral loop and rostral approach to the mandibular division of the trigeminal nerve (Figure 14). The bend in the paths taken by the branches of the facial nerve become more defined during ontogeny in response to the lengthening of the skull and brain in the adult.

3.9 | Cranial nerve VIII: Vestibulocochlear

The vestibulocochlear nerve (CN VIII) transmits only sensory signals and extends laterally from the pontine-medulla junction, just caudal to the root of the facial nerve (Figures 2 and 12). The vestibular divisions (nV) and the cochlear branch (nC) pass through individual foramina (fCN VIII) on the medial surface of the prootic before extending to the ampullae of the semicircular canals (nAc, nAl, nAr) and cochlea, respectively (Figures 7 and 12). In the larger specimens, the vestibulocochlear branches are shorter and less defined as the middle and inner ear increase in size and proximity to the root of the nerve.

3.10 | Cranial nerve IX: Glossopharyngeal

The glossopharyngeal nerve (CN IX) transmits both motor and sensory signals and originates from the medulla, extending laterally to exit the cranial cavity via the jugular foramen (fCN IX) in the exoccipital (Figures 2, 7, 9, and 12). Just after exiting the jugular foramen, it forms the petrosal ganglion (IX_g) then extends ventrally passing by the external carotid artery. Extending further ventrally, the glossopharyngeal nerve passes along the dorsal border of the *m. constrictor colli profundus* and between the *m. branchiohyodieus dorsalis* (mBHd) and *m. branchiohyoideus ventralis* (mBHv) (Figure 15) (innervating these two; Li & Clarke, 2015) and lateral to the hyoid. Then it passes medial to the *m. geniohyoideus* (mGH) to the ventral border of the tongue. This nerve takes an increasingly tortuous path to its destinations during ontogeny in response to the increasingly horizontal orientation of the hindbrain.

3.11 | Cranial nerve X: Vagus

The vagus nerve (CN X) transmits both motor and sensory signals and originates from the medulla extending laterally to exit the cranial cavity via the jugular foramen (fCN X) in the exoccipital (Figures 2, 7, 9, and 12). Just after exiting the jugular foramen, it forms a ganglion (dorsal to the sympathetic ganglion [S_g], the jugular and/or nodose ganglion, X_g) before passing ventrally with the internal carotid. The vagus nerve then takes a tortuous ventral path medial to the glossopharyngeal nerve before splitting at the dorsal extent of the *m. constrictor colli profundus* (Li & Clarke, 2015). The pharyngolaryngeal branch (of Shiino, 1914, nPHL) passes rostrally, medial to the *m. constrictor colli profundus* and medial to the hyoid along the dorsal border of the *m. omohyoideus* (Li & Clarke, 2015). Then the pharyngolaryngeal branch passes medially, ventral to the *m. constrictor larynges* (mCL) and the m. cricoarytenoid (Figure 16, mCR) (innervating them; see Riede et al., 2015 for laryngeal musculature details). The vagal branch (of Shiino, 1914) extends caudally from the division alongside the lateral border of the esophagus into the thorax. Like the glossopharyngeal nerve, the vagus nerve also takes an increasingly tortuous path to its destinations as specimen size increases in response to the increasingly horizontal orientation of the hindbrain.

3.12 | Cranial nerve XI: Accessory

We skip discussion of the accessory nerve as it originates outside of the skull from cervical nerve roots and targets cervical musculature and is therefore, though passing through the jugular foramen from the cranial cavity, not a "cranial" nerve (Benninger & McNeil, 2010).

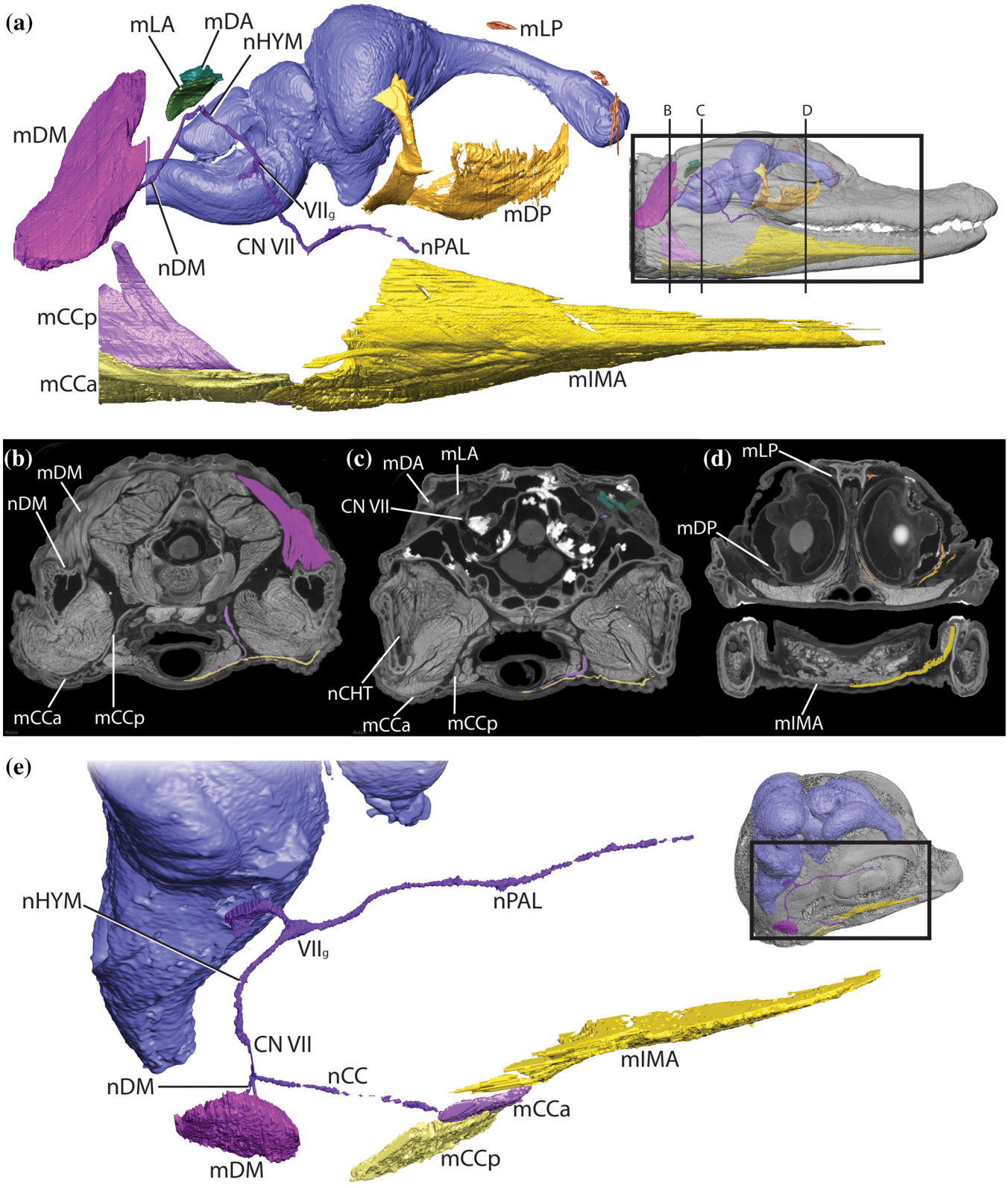

FIGURE 13 Facial Nerve-Innervated Muscles. 3D reconstruction of the brain, cranial nerve VII, the facial nerve-innervated muscles, and head of yearling alligator MUVC AL031 (a) and stage 19 embryo MUVC AL031 (e) in right lateral (a) and right dorsolateral views (b) with axial CT slices of MUVC AL031 (b–d). A 3D model of (a) may be found at: https://sketchfab.com/3d-models/yearling-alligator-cn-vii-innervated-muscles-c2d269b76ef9402480ab296feda0f675 and a 3D model of (e) may be found at: https://sketchfab.com/3d-models/embryonic-alligator-cn-vii-innervated-muscles-278d5ba701ff43aa898915e52ae049c7

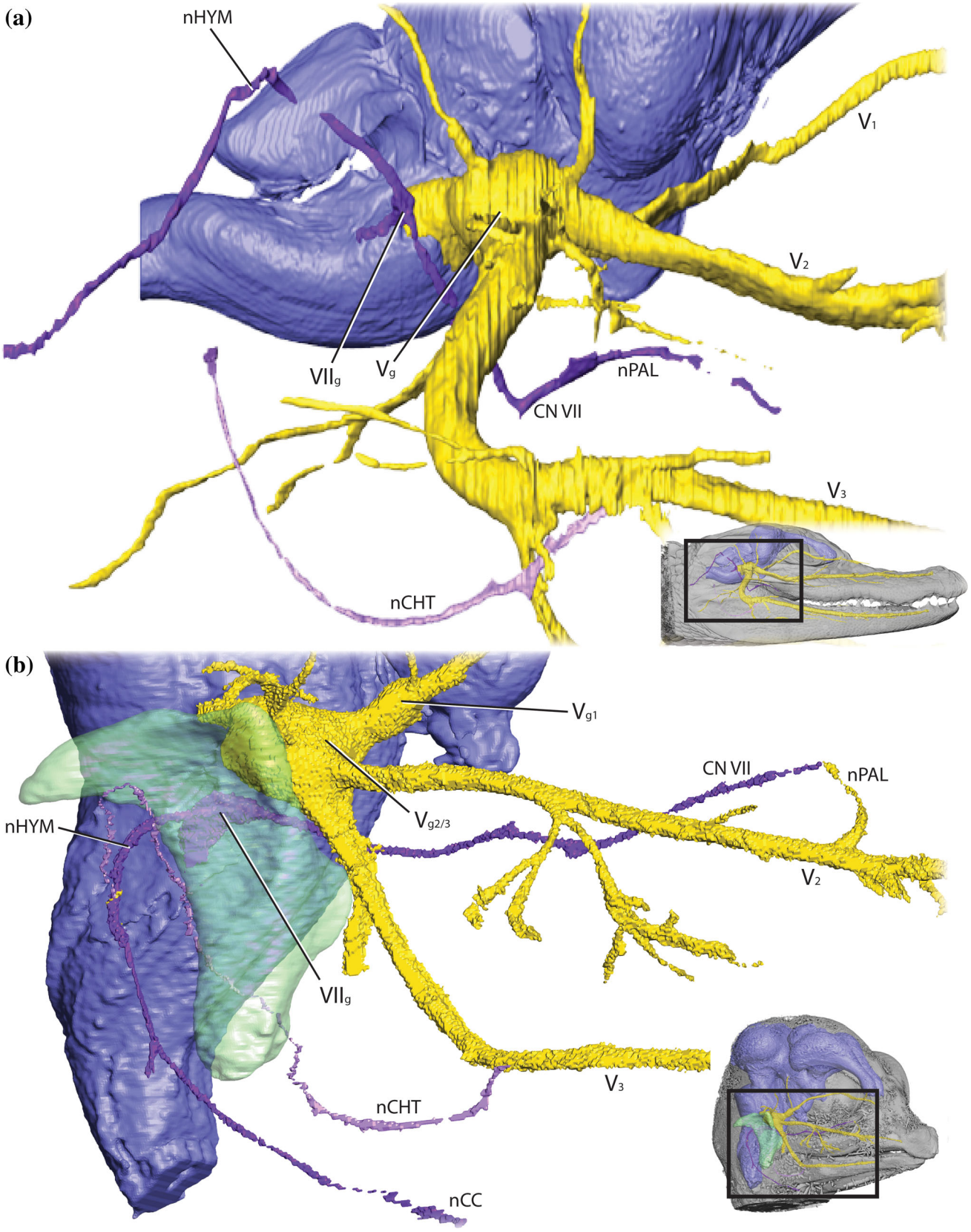

FIGURE 14 Chorda Tympani. 3D reconstruction of the brain, cranial nerves V and VII, potential path of the chorda tympani branch of CN VII, and head of yearling alligator MUVC AL031 (a) and embryo MUVC AL089 (b, mirrored) in right lateral (a) and right rostrolateral (b) views. Developing quadrate is included in green for the embryonic alligator (b)

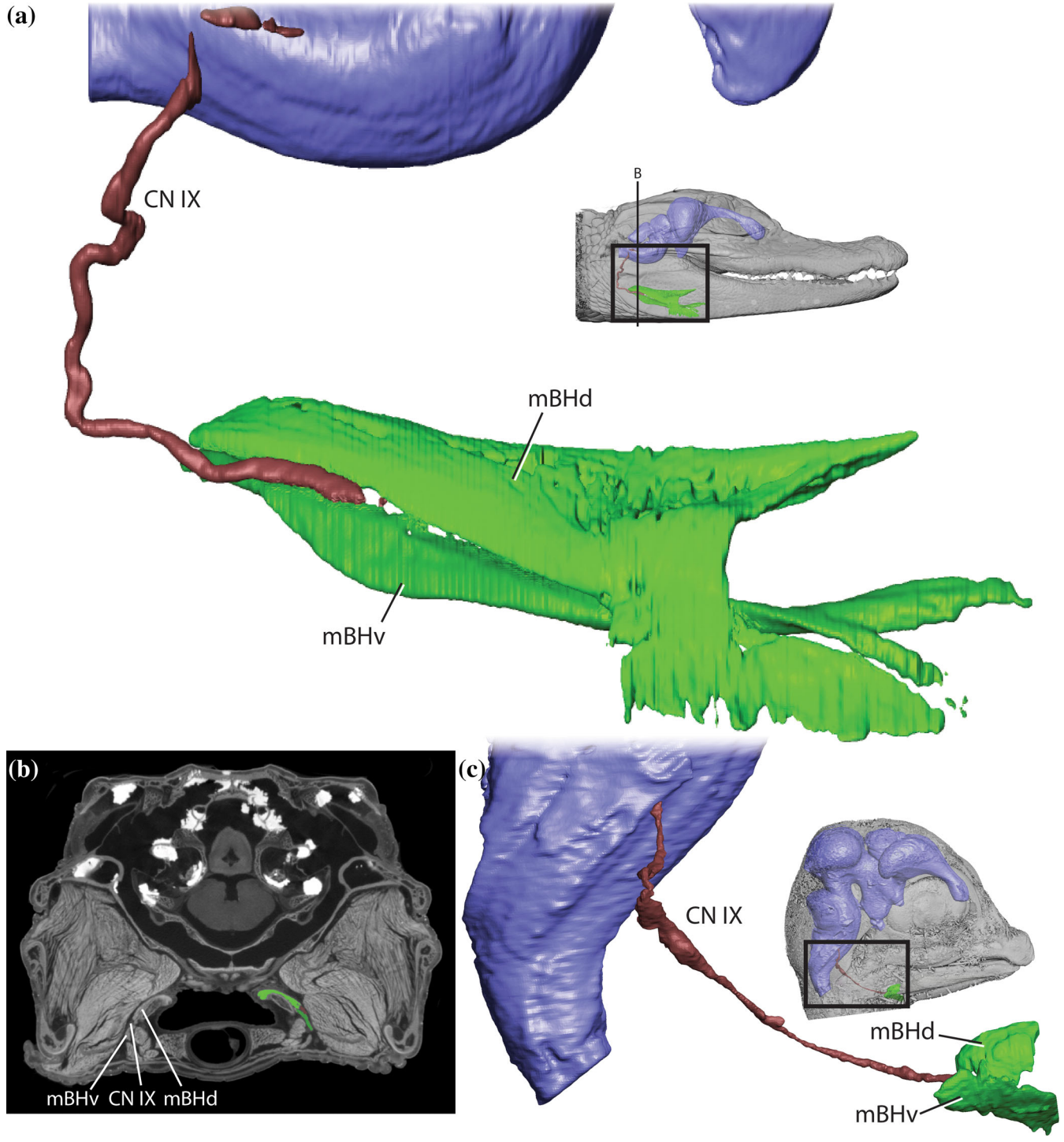

FIGURE 15 Glossopharyngeal Nerve-Innervated Muscles. 3D reconstruction of the brain, head, cranial nerve IX, and glossopharyngeal nerve-innervated muscles of yearling alligator MUVC AL031 (a) and stage 19 embryo MUVC AL089 (C, mirrored) in right lateral view with an axial CT slice (b). (Colors follow Li & Clarke, 2015). A 3D model of (a) may be found at: https://sketchfab.com/3d-models/yearling-alligator-cn-ix-innervated-muscles-fd0d25c386494e719ca17cc742e76443 and a 3D model of (c) may be found at: https://sketchfab.com/3d-models/embryonic-alligator-cn-ix-innervated-muscles-61720901bf684060aa0c1fba74475f5e

3.13 | Cranial nerve XII: Hypoglossal

The hypoglossal nerve (CN XII) transmits motor signals and originates from the medulla and extends laterally through the hypoglossal foramen (fCN XII) in the exoccipital (Figures 2, 7, 9, and 12). The hypoglossal nerve passes rostral to the first cervical nerve before extending ventrally through the *m. longissimus capitis*

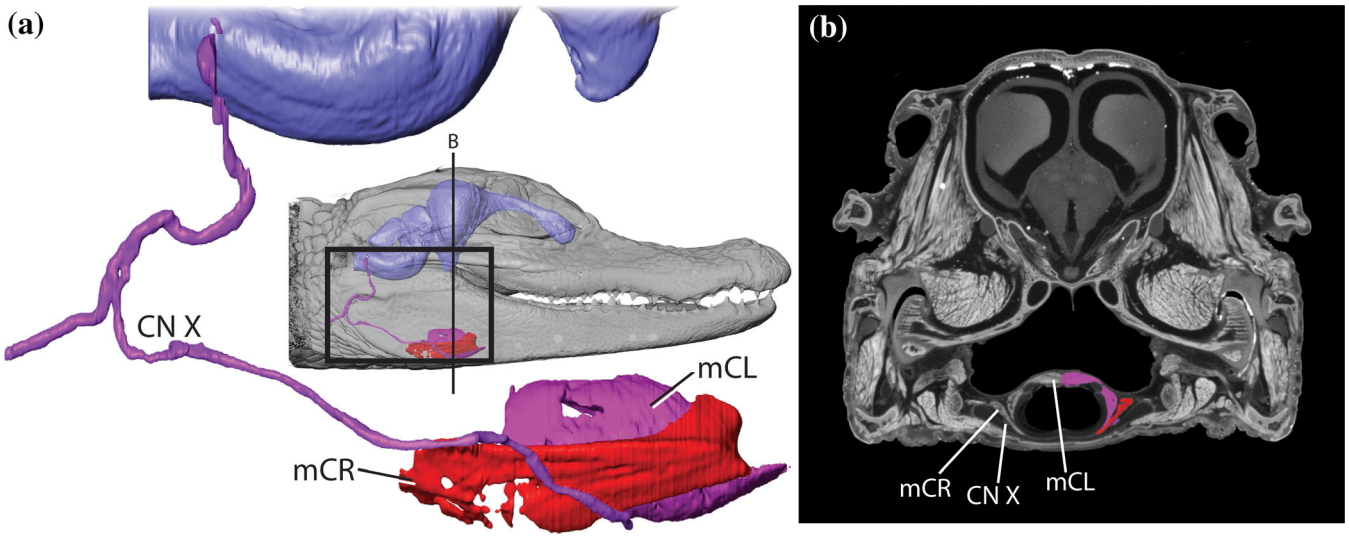

FIGURE 16 Vagus Nerve-Innervated Muscles. 3D reconstruction of the brain, head, cranial nerve X, and vagus nerve-innervated muscles of yearling alligator MUVC AL031 (a) in right lateral view with an axial CT slice (b). (Colors follow Riede, Li, Tokuda, & Farmer, 2015). A 3D model of (a) may be found at: https://sketchfab.com/3d-models/yearling-alligator-cn-x-innervated-muscles-c05d83b85d6247c1a97f360f144c5c37

(Al-Hassawi, 2004). From there, it follows a tortuous path, paralleling the vagus nerve medial to the *m. constrictor colli profundus* before turning rostrally at the dorsal extent of the *m. omohyoideus* (Li & Clarke, 2015). The hypoglossal nerve then extends rostrolaterally, paralleling the glossopharyngeal nerve lateral to the hyoid and medial to the *m. branchiohyoideus dorsalis* (Li & Clarke, 2015). The nerve continues rostrally along the floor of the mouth, innervating the *m. hyoglossus* (mHG), *m. genioglossus* (mGG), *m. geniohyoideus* (mGH), *m. episternobranchiotendineus* (mEBT) and the *m. episternobranchialis* (Figure 17, mEB) (see Li & Clarke, 2015) before anastomosing with the opposing hypoglossal nerve at the level of the fourteenth dentary tooth (counted from rostral). The hypoglossal nerve has numerous caudal extensions (nCV) before its rostrolateral curve, which extend to meet the cervical nerves. The hypoglossal nerve, like the glossopharyngeal and vagus nerves, increases in tortuosity during ontogeny in response to the increasingly horizontal orientation of the hindbrain.

3.14 | Cranial autonomic nerves

The autonomic system is discussed here because of its many cranial targets and shared pathways with cranial nerves. Where nerves are untraceable in these data, this description relies on that of Shiino (1914) and Bellairs and Shute (1953, esp. Text-Figure 5.).

The most evident autonomic nerves in the alligator cranium are those of the sympathetic system. The sympathetic nerve (nSYM) travels cranially lateral to the cervical vertebrae until forming a sympathetic ganglion (S_g) just outside the jugular foramen (Bellairs & Shute, 1953; Shiino, 1914). The ganglion is in close contact with the petrosal ganglion of the glossopharyngeal nerve and the vagus ganglion of the vagus nerve (Figures 4, 5, 9, and 12). From there, the thick cranial sympathetic nerve extends through the jugular foramen into the exoccipital, around the round window of the otic capsule, across the secondary tympanic membrane, medial to the facial nerve, around the lateral semicircular duct, dorsal to the geniculate ganglion to the maxillomandibular ganglion of the trigeminal nerve (Bellairs & Shute, 1953). Bellairs and Shute (1953) reported a communicating branch to the hyoid ramus of the facial nerve (too small to see in these data) which ultimately innervates the *m. constrictor colli profundus*, *m. levator auriculae*, *m. depressor auriculae*, *m. levator palpebrae* (mLP), and *m. depressor palpebrae* (Figure 13, mDP). The sympathetic nerve contacts the maxillomandibular ganglion of the trigeminal nerve, and in our dataset, further branches are not visible. Bellairs and Shute (1953) reported communicating branches with the maxillomandibular and ophthalmic ganglia and nerves that travel with the ophthalmic nerve eventually innervating the nasal gland and narial muscles via the lateral nasal (ethmoidal) ramus (Figure 10, nN). The sympathetic nerve is large in diameter in the embryo, but too small to locate in the yearling and adult specimens.

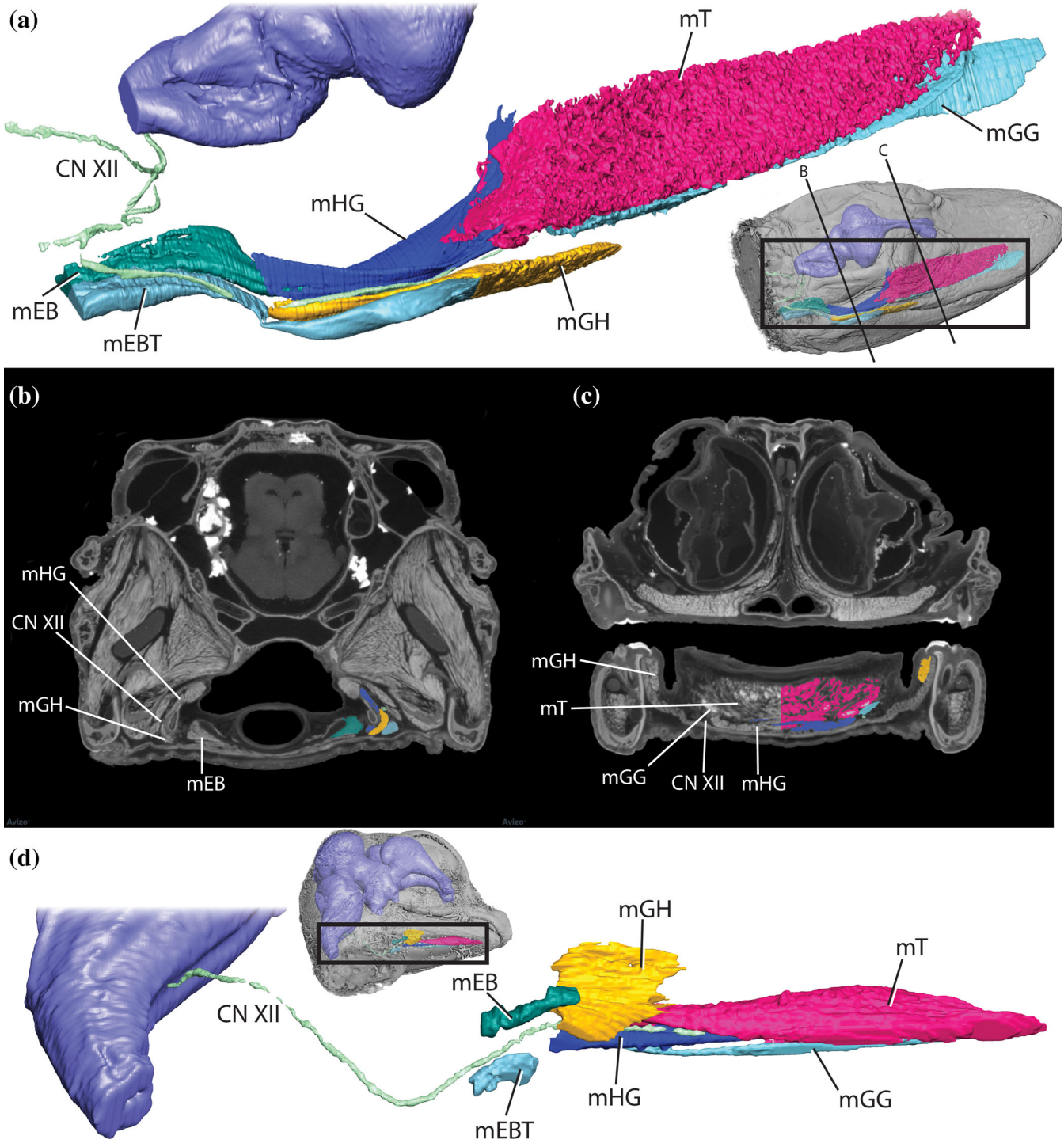

FIGURE 17 Hypoglossal Nerve-Innervated Muscles. 3D reconstruction of the brain, head, cranial nerve XII, and the hypoglossal-innervated muscles of yearling alligator MUVC AL031 in right dorsolateral view (a) and stage 19 embryo MUVC AL089 in right ventrolateral view (d, mirrored) with axial CT slices of MUVC AL031 (b, d). (Colors follow Li & Clarke, 2015). A 3D model of (a) may be found at: https://sketchfab.com/3d-models/yearling-alligator-cn-xii-innervated-muscles-f116e8e8222d4607a998107d06e45f50 and a 3D model of (d) may be found at: https://sketchfab.com/3d-models/embryonic-alligator-cn-xii-innervated-muscles-764fd8ced1e545668930938b39dd9de5

The alligator parasympathetic nervous system is represented by three ganglia along the course of cranial nerves (Bellairs & Shute, 1953). The oculomotor nerve holds the ciliary ganglion (C_g) just caudal to the branch to the *m. rectus dorsalis* (Figures 3 and 4). The parasympathetic nerves of the ciliary ganglion innervate the

ciliary and sphincter muscles responsible for focusing the eye via constricting the pupil and adjusting the lens. The maxillary division of the trigeminal nerve holds the palatine ganglion (P_g) rostrally, at the location of a communicating branch with the palatine division of the facial nerve (Figure 4). These two ganglia are evident in the embryonic alligator, but not visible in the yearling or adult specimens. The parasympathetic nerves of the palatine ganglion innervate the orbital glands and mucosa of the nasal cavity and palate. Bellairs and Shute (1953) reported a mandibular (submandibular) ganglion along the chorda tympani but the presence of this ganglion is unclear in these data. The parasympathetic nerves of the mandibular ganglion innervate the submandibular and sublingual glands.

4 | DISCUSSION

This study provides a three-dimensional view of alligator cranial nerve anatomy. It adds to the growing collection of 3D alligator data and those of other crocodylians (e.g., Dufeau & Witmer, 2015; Holliday et al., 2013; Li & Clarke, 2015; Porter et al., 2016; Riede et al., 2015; Rowe et al., 1999) also contributing to the numerous imaging resources available for download. Also, data from extant

TABLE 2 Individual URLs to 3D models of figures found in the Sketchfab collection (https://sketchfab.com/holliday/collections/alligator-cranial-nerve-atlas)

Figure(s)	URL
5A	https://sketchfab.com/3d-models/yearling-alligator-extraocular-muscles-832ea36447394124b9fa51fbed6bcd9b
5D	https://sketchfab.com/3d-models/embryonic-alligator-extraocular-muscles-03ccd7cc21fd40608d6bb4dbd6e61578
6	https://sketchfab.com/3d-models/embryonic-alligator-cranial-nerves-b14a75f97da74cd89e402d118ba38e59
7B and 9A	https://sketchfab.com/3d-models/alligator-skull-and-cranial-nerves-98c9ca48f3a3408f8c64d6c6d4256aee
11A	https://sketchfab.com/3d-models/yearling-alligator-cn-v-innervated-muscles-538568dea57041628e8a5b564b30b2eb
11D	https://sketchfab.com/3d-models/embryonic-alligator-cn-v-innervated-muscles-3a7d93f76545415da07e60d46d03c346
13A	https://sketchfab.com/3d-models/yearling-alligator-cn-vii-innervated-muscles-c2d269b76ef9402480ab296feda0f675
13E	https://sketchfab.com/3d-models/embryonic-alligator-cn-vii-innervated-muscles-278d5ba701ff43aa898915e52ae049c7
15A	https://sketchfab.com/3d-models/yearling-alligator-cn-ix-innervated-muscles-fd0d25c386494e719ca17cc742e76443
15C	https://sketchfab.com/3d-models/embryonic-alligator-cn-ix-innervated-muscles-61720901bf684060aa0c1fba74475f5e
16A	https://sketchfab.com/3d-models/yearling-alligator-cn-x-innervated-muscles-c05d83b85d6247c1a97f360f144c5c37
17A	https://sketchfab.com/3d-models/yearling-alligator-cn-xii-innervated-muscles-f116e8e8222d4607a998107d06e45f50
17D	https://sketchfab.com/3d-models/embryonic-alligator-cn-xii-innervated-muscles-764fd8ced1e545668930938b39dd9de5
3B, 5A, 10B, 11A, 12B, 13A, 14A, 15A, 16A, 17A	https://sketchfab.com/3d-models/yearling-alligator-cranial-nerves-and-muscles-6563d92576ab475ca31f2752ea710248
3B, 10B, 12B, 14A	https://sketchfab.com/3d-models/yearling-alligator-cranial-nerves-51dbdca420454effb324a88753b047f9
3C, 5D, 6, 10C, 11D, 12C, 13E, 14B, 15C, 17D	https://sketchfab.com/3d-models/embryonic-alligator-cranial-nerves-and-muscles-3c844a3b122044c6b533ac2de8a5fb7b

Note: Load model URL into the model inspector (https://labs.sketchfab.com/experiments/model-inspector) to toggle layers using "Scene."

taxa provide detailed, necessary phylogenetic brackets for the increasingly common studies of paleoneurology from endocasts of extinct pseudosuchian species (e.g., Mastrantonio, von Baczko, Desojo, & Schultz, 2019; Sereno & Larsson, 2009; von Baczko, Taborda, & Desojo, 2018). These datasets are available from Sketchfab as annotated, 3D interactive models (see Table 2) (https://sketchfab.com/holliday/collections/alligator-cranial-nerve-atlas). Sketchfab also provides a model inspector (https://labs.sketchfab.com/experiments/model-inspector) in which model objects may be toggled on or off using "Scene" to further explore structure relationships in three dimensions. Raw datasets are available when possible from Open Science Framework (https://osf.io/jmpck/).

4.1 | Anatomy

Overall, there are not many gross anatomical differences among alligator cranial nerves at these ontogenetic stages. The absence of differences is itself significant. Any changes occur largely as a result of the changing skull and brain shapes during ontogeny. The cranial nerves are brought along as they maintain their pathway from origin to destination. The cranial modules grow at different rates (Goswami, 2006; Watanabe et al., 2019), yet the cranial nerves maintain their origins and targets during development regardless of the distance between (Vogel, 1992). At stage 19 in the alligator the placode-derived sensory neurons have all contacted the hindbrain and their targets. As the hindbrain becomes horizontal and the skull elongates, the trigeminal, facial, glossopharyngeal, vagus, and hypoglossal nerves all must grow at a faster rate than the nerves to the ears, eye, and extraocular muscles. The olfactory nerve maintains close contact between the olfactory bulbs and the nasal mucosa and therefore grows at the slowest rate.

There are some noteworthy differences with respect to the trigeminal nerve among datasets. The embryonic specimen has two distinct ganglia (i.e., ophthalmic [profundal] and maxillomandibular [Gasserian]) that have not yet fused into a single trigeminal ganglion at stage 19, day 27–28 of in ovo development, rather than a single-fused trigeminal ganglion as seen in the yearling and adult specimens. With more embryonic sampling, it will be possible to pinpoint the developmental stage at which these ganglia merge, adding a character not typically used in embryonic staging, though potentially useful in evolutionary and developmental neurological comparisons. The trigeminal nerve ganglion also increases in size with respect to the brain during ontogeny, perhaps tied to the increase in diameter of the maxillary and mandibular divisions in comparison to the ophthalmic division. The maxillary and mandibular regions receive sensory input from most of the rostral sensory organs, which are responsible for fine sensation and orientation to prey (Leitch & Catania, 2012). Increase in nerve and ganglion size implies an increase in myelination of neurons, which leads to an increase in signal propagation, and therefore faster sensory speeds and increased performance in larger specimens (Kandel, Schwart, & Jessell, 2000). This is supported by the observation of George and Holliday (2013) that axon density decreases in larger alligators, likely because myelin sheaths increase in size. We suspect that histological investigation of the merged trigeminal ganglia would show a larger increase in maxillomandibular ganglion size than ophthalmic ganglion size during alligator ontogeny.

Another noteworthy difference between the embryonic and larger individuals is the increasing tortuosity of the glossopharyngeal, vagus, and hypoglossal nerves. These likely reflect the extra length of nerve required for the range of head movements alligators engage in and therefore, with the elastic properties of nerves (e.g., Vogl et al., 2015), could be used as constraints in biomechanical investigations of head orientation, gape, and other movements.

These data show a single cranial sympathetic ganglion (the rostral [superior] cervical ganglion, S_g), even in the embryonic specimen. This is actually a fusion of the primary and secondary cervical ganglia (Bellairs & Shute, 1953; Shiino, 1914), only visible using histology. These two ganglia ultimately fuse with the petrosal (IX_g) and vagus (X_g) ganglia during ontogeny. As with the fusion of the trigeminal ganglia, pinpointing the developmental stage at which these ganglia merge could be a potentially useful character for comparison across reptiles. Reptilian autonomic systems are not well researched in general, so unraveling sympathetic distribution along the other cranial nerves is the first step in understanding autonomic components of cranial nerves and autonomic function in the reptile head.

4.2 | Homology

Nerve homology guides our understanding of the origins of cranial bones, dermatomes, muscles, glands, and other structures. Nerves and their branches maintain conserved pathways through structures, and tracing nerves and their branches from origin to target through development is a successful method of testing for structure homology (e.g., trigeminal nerve and jaw muscle topology

[Holliday & Witmer, 2007] and the hypoglossal nerve and craniocervical homology [Maddin, Piekarski, Reis, & Hanken, 2020]). Data provided here can further understanding of homologous structures and their evolutionary and developmental origins. Cranial element homology is usually traced by fate mapping of embryonic precursors (e.g., Maddin, Piekarski, Sefton, & Hanken, 2016), but nerves with identical origins could be traced to targets of questionable origin. Also, it has been suggested that the skull roof tracks with the brain during evolution and development in reptiles (Fabbri et al., 2017), but it may also track with cranial nerve innervation. Similarly, as suggested by Holliday and Witmer (2007), there are conserved muscle groups traceable through trigeminal motor nerves and conserved trigeminal dermatomes traceable through trigeminal sensory nerves. For example, the integument over the interorbital region, formed by the frontal bone, is innervated by the frontal branch of the ophthalmic division of the trigeminal nerve in the alligator, whereas the integument over the postorbital region, formed by the frontal, postorbital, and parietal bones, is innervated by the supraorbital ramus of the maxillary division of the trigeminal nerve. Therefore, homologous nerves are expected to arise from the ophthalmic and maxillary divisions in other taxa and would distinguish between homologous regions (e.g., interorbital vs. postorbital) and elements (e.g., frontal vs. postorbital vs. parietal) in those taxa. The other sensory nerves should follow similar patterns, defining homologous muscle groups and sensory regions when explored across multiple taxa. Finally, the origins of cranial glands are often discussed (e.g., Fry et al., 2006; Jarrar & Taib, 1987; Kardong, Weinstein, & Smith, 2009) especially when investigating origins of venom (e.g., Fry et al., 2012; McDowell, 1986), and nerve innervation (by autonomic nerves along CN VII or CN V) is a possible method to confirm homology.

4.3 | Methods

This study highlights both the utility and drawbacks of contrast-enhanced CT imaging and 3D reconstruction. Numerous structures of various tissue types (e.g., muscle, bone, nerve, including both myelinated (e.g., CN V) and unmyelinated (CN I) nerves, were identified in multiple specimens of various sizes making it possible to track growth and development of structures. The interconnected anatomy of the flat crocodylian skull is difficult to approach in traditional dissection, and this method allows for a nondestructive view into a complex region. Unfortunately, though resolution has increased since CT scanning for anatomical purposes began in the late 20th century, it is still one of the largest limiting factors. Many finer nerve branches that supply muscles or are parts of the autonomic system are still only visible using histology and sometimes dissection. These branches remain missing from this CT data either because these branches are too fine for contrast particles to bind to or because the specimens were scanned with a lower resolution than necessary to see them. Similarly, thin muscles with few muscle fascicles are also not visible with this method. Specific examples in this dataset include the *m. constrictor internus dorsalis* (mCID) and the trigeminal ramus that innervates these muscles (nCID), the trigeminal ramus (nCCa) to the *m. constrictor colli pars anterior* (mCCa), the *m. quadratus* (muscle of the nictitating membrane) and its motor ramus from the abducens nerve, and communicating branches from the sympathetic nerve to other cranial nerves. However, in the case that branches are missing from a dataset, occasionally, they were discernible in another, such as the case with the frontal branch (nFR) from the trigeminal nerve and the sympathetic nerve (nSYM), which were only visible in the embryonic dataset. This method of contrast is also limited in highlighting the vasculature accompanying nerves and supplying structures. Finally, details on the cellular level are absent and require complementary histology to visualize, such as fiber decussation in the optic chiasm, distinction between fused ganglia, somatotopy, axon counts, and extent of myelination.

We also caution against drawing conclusions before careful comparison of 3D-reconstructed data and dissected and histologically processed specimens. When presented with such a large amount of complicated structures, familiarization with 3D relationships can prove difficult to untangle and misidentification is quite easy. Before structure identification, it is necessary to explore the structure from origin to target and confirm its topological relationships with other structures (often conserved) with the literature, dissection, and other available 3D resources.

ACKNOWLEDGMENTS

The authors thank Ruth Elsey and the Rockefeller State Refuge and Missouri Animal Care & Use Committee for aid in procuring and housing alligators. Thanks to Tara Selly, Jim Schiffbauer, and MizzoμX, and Ashley Szydrozski, Tim Hoffman, and the Biomolecular Imaging Center, and Jessie Maisano, Matt Colbert, and UTCT for CT scanning.

AUTHOR CONTRIBUTIONS

Emily J. Lessner: data collection, investigation, and writing. **Casey Holliday:** Funding acquisition; investigation; resources; software; writing-review and editing.

ORCID

Emily J. Lessner https://orcid.org/0000-0003-0774-1613
Casey M. Holliday https://orcid.org/0000-0001-8210-8434

REFERENCES

Al-Hassawi AMA. The osteology and myology of the craniocervical region in squamate reptiles: a comparative study. PhD dissertation, University College London; 2004.

Allen, V., Elsey, R. M., Jones, N., Wright, J., & Hutchinson, J. R. (2010). Functional specialization and ontogenetic scaling of limb anatomy in *Alligator mississippiensis*. *Journal of Anatomy*, *216*, 423–445.

Bellairs, A. A., & Shute, C. C. D. (1953). Observations on the narial musculature of Crocodilia and its innervation from the sympathetic system. *Journal of Anatomy*, *87*, 367–378.

Benninger, B., & McNeil, J. (2010). Transitional nerve: A new and original classification of a peripheral nerve supported by the nature of the accessory nerve (CN XI). *Neurology Research International*, *2010*, 1–15.

Busbey, A. B., III. (1989). Form and function of the feeding apparatus of *Alligator mississippiensis*. *Journal of Morphology*, *202*, 99–127.

Carlisle A, Weisbecker V. 2016. A modified STABILITY protocol for accurate retrieval of soft-tissue data from micro-CT scans of IKI-stained specimens. Published online at https://dicect.com/2016/08/09/stability/, August 9, 2016.

Colbert, E. H., Cowles, R. B., & Bogert, C. M. (1946). Temperature tolerances in the American alligator and their bearing on the habits, evolution, and extinction of the dinosaurs. *Bulletin of the AMNH*, *86*, 333–373.

Crosby, E. C. (1917). The forebrain of *Alligator mississippiensis*. *Journal of Comparative Neurology*, *27*, 325–402.

Cunningham, S., Castro, I., & Alley, M. (2007). A new prey-detection mechanism for kiwi (*Apteryx spp.*) suggests convergent evolution between paleognathous and neognathous birds. *Journal of Anatomy*, *211*, 493–502.

Dodson, P. (1975). Functional and ecological significance of relative growth in *Alligator*. *Journal of Zoology (London)*, *175*, 315–355.

Dufeau, D. L., & Witmer, L. M. (2015). Ontogeny of the middle-ear air-sinus system in *Alligator mississippiensis* (Archosauria: Crocodylia). *PLoS One*, *10*, 1–25.

Erickson, G. M., Lappin, A. K., & Vliet, K. A. (2003). The ontogeny of bite-force performance in American alligator (*Alligator mississippiensis*). *Journal of Zoology*, *260*, 317–327.

Fabbri, M., Koch, N. M., Pritchard, A. C., Hoffman, E., Bever, G. S., Balanoff, A. M., ... Rowe, T. B. (2017). The skull roof tracks the brain during the evolution and development of reptiles including birds. *Nature Ecology and Evolution*, *1*, 1543–1550.

Ferguson, M. W. J. (1984). Craniofacial development in Alligator mississippiensis. The structure, development and evolution of reptiles. M. W. J. Ferguson *The Structure, Development and Evolution of Reptiles, Symposia of the Zoological Society of London*, 52, 223–273. New York: Academic Press.

Ferguson, M. W. J. (1985). Reproductive biology and embryology of the crocodilians. In C. Gans, F. Billet, & P. F. A. Maderson (Eds.), *Biology of the Reptilia* (Vol. 14, pp. 329–491). New York: Wiley.

Fry, B. G., Vidal, N., Norman, J. A., Vonk, F. J., Scheib, H., Ramjan, S. R., ... Hodgson, W. C. (2006). Early evolution of the venom system in lizards and snakes. *Nature*, *439*, 584–588.

Fry, B. G., Casewell, N. R., Wüster, W., Vidal, N., Young, B., & Jackson, T. N. (2012). The structural and functional diversification of the Toxicofera reptile venom system. *Toxicon*, *60*, 434–448.

George, I. D., & Holliday, C. M. (2013). Trigeminal nerve morphology in *Alligator mississippiensis* and its significance for crocodyliform facial sensation and evolution. *The Anatomical Record*, *296*, 670–680.

Gignac, P. M., & Erickson, G. M. (2016). Ontogenetic bite-force modeling of *Alligator mississippiensis*: Implications for dietary transitions in a large-bodied vertebrate and the evolution of crocodylian feeding. *Journal of Zoology*, *299*, 229–238.

Goodrich, E. S. (1915). Memoirs: The chorda tympani and middle ear in reptiles, birds, and mammals. *Journal of Cell Science*, *2*, 137–160.

Goswami, A. (2006). Cranial modularity shifts during mammalian evolution. *The American Naturalist*, *168*, 270–280.

Hansen, A. (2007). Olfactory and solitary chemosensory cells: Two different chemosensory systems in the nasal cavity of the American alligator, *Alligator mississippiensis*. *BMC Neuroscience*, *8*, 1–10.

Hieronymus, T. L., & Witmer, L. M. (2010). Homology and evolution of avian compound rhamphothecae. *The Auk*, *127*, 590–604.

Holliday, C. M., & Witmer, L. M. (2007). Archosaur adductor chamber evolution: Integration of musculoskeletal and topological criteria in jaw muscle homology. *Journal of Morphology*, *268*, 457–484.

Holliday, C. M., & Witmer, L. M. (2009). The epipterygoid of crocodyliforms and its significance for the evolution of the orbitotemporal region of eusuchians. *Journal of Vertebrate Paleontology*, *29*, 715–733.

Holliday, C. M., Tsai, H. P., Skiljan, R. J., George, I. D., & Pathan, S. (2013). A 3D interactive model and atlas of the jaw musculature of *Alligator mississippiensis*. *PLoS One*, *8*, e62806.

Hotton, N. (1960). The chorda tympani and middle ear as guides to origin and divergence of reptiles. *Evolution*, *14*, 194–211.

Iordansky, N. N. (1964). The jaw muscles of the crocodiles and some relating structures of the crocodilian skull. *Antomischer Anzeiger*, *115*, 256–280.

Iordansky, N. N. (1973). The skull of the Crocodilia. In C. Gans (Ed.), *Biology of the Reptilia, Vol. 4: Morphology D* (pp. 201–262). New York: Academic Press.

Jollie, M. (1962). *Chordate morphology*. New York: Reinhold Publishing Co.

Kandel, E., Schwart, J., & Jessell, T. (2000). *Principals of neural science* (fourth ed.). New York: McGraw-Hill.

Jarrar, B. M., & Taib, N. T. (1987). The Histochemistry of the labial salivary glands of the spiny-tailed lizard *Uromastyx microlepis* (Blandford). *Amphibia-Reptilia*, *8*, 59–67.

Kardong, K. V., Weinstein, S. A., & Smith, T. L. (2009). Reptile venom glands: Form, function, and future. S. Mackessy In *Handbook of venoms and toxins of reptiles* (pp. 65–91). Boca Raton, Florida: CRC Press.

Klembara, J. (2001). Postparietal and prehatching ontogeny of the supraoccipital in *Alligator mississippiensis* (Archosauria, Crocodylia). *Journal of Morphology*, *249*, 147–153.

Lakjer, T. (1926). *Studien über die Trigeminus-versorgte Kaumuskulatur der Sauropsiden.* Copenhagen, Denmark: CA Reitzel.

Leitch, D. B., & Catania, K. C. (2012). Structure, innervation and response properties of integumentary sensory organs in crocodilians. *The Journal of Experimental Biology*, *215*, 4217–4230.

Lessner, E. J., Gant, C. A., Hieronymus, T. L., Vickaryous, M. K., & Vickaryous, C. M. (2019). Anatomy and ontogeny of the mandibular symphysis in Alligator mississippiensis. *The Anatomical Record*, *302*(10), 1696–1708. https://doi.org/10.1002/ar.24116.

Li, Z., & Clarke, J. A. (2015). New insight into the anatomy of the hyolingual apparatus of *Alligator mississippiensis* and implications for reconstructing feeding in extinct archosaurs. *Journal of Anatomy*, *227*, 45–61.

Maddin, H. C., Piekarski, N., Sefton, E. M., & Hanken, J. (2016). Homology of the cranial vault in birds: New insights based on embryonic fate-mapping and character analysis. *Royal Society Open Science*, *3*, 160356.

Maddin, H. C., Piekarski, N., Reis, R. R., & Hanken, J. (2020). Development and evolution of the tetrapod skull–neck boundary. *Biological Reviews*, *95*, 573–591.

Mastrantonio, B. M., von Baczko, M. B., Desojo, J. B., & Schultz, C. L. (2019). The skull anatomy and cranial endocast of the pseudosuchid archosaur *Prestosuchus chiniquensis* from the Triassic of Brazil. *Acta Palaeontologica Polonica*, *64*, 171–198.

McDowell, S. B. (1986). The architecture of the corner of the mouth of colubroid snakes. *Journal of Herpetology*, *20*, 353–407.

Monteiro, L. R., Cavalcanti, M. J., & Sommer, H. J. S., III. (1997). Comparative ontogenetic shape changes in the skull of caiman species (Crocodylia, Alligatoridae). *Journal of Morphology*, *231*, 53–62.

Müller, G. B., & Alberch, P. (1990). Ontogeny of the limb skeleton in *Alligator mississippiensis*: Developmental invariance and change in the evolution of archosaur limbs. *Journal of Morphology*, *203*, 151–164.

Poglayen-Neuwall, I. (1953). Untersuchungen der Kiefermuskulatur und deren Innervation an Krokodilen. *Anatomischer Anzeiger*, *99*, 257–296.

Porter, W. R., Sedlmayr, J. C., & Witmer, L. M. (2016). Vascular patterns in the heads of crocodilians: Blood vessels and sites of thermal exchange. *Journal of Anatomy*, *229*, 800–824.

Reese, A. M. (1915). *The alligator and its allies*. New York: GP Putnam's Sons.

Riede, T., Li, Z., Tokuda, I. T., & Farmer, C. G. (2015). Functional morphology of the *Alligator mississippiensis* larynx with implications for vocal production. *The Journal of Experimental Biology*, *218*, 991–998.

Rieppel, O. (1993). Studies on skeleton formation in reptiles. V. Patterns of ossification in the skeleton of *Alligator mississippiensis* DAUDIN (Reptilia, Crocodylia). *Zoological Journal of the Linnean Society*, *109*, 301–325.

Romer, A. S. (1956). *Osteology of the reptiles*. Chicago: The University of Chicago Press.

Rowe, T., Brochu, C. A., Colbert, M., Merck, J. W., Kishi, K., Saglamer, E., & Warren, S. (1999). Introduction to alligator: Digital atlas of the skull. *Journal of Vertebrate Paleontology*, *19*, 1–8.

Schumacher, G. H. (1973). The head muscles and hyolaryngeal skeleton of turtles and crocodilians. In C. Gans & T. S. Parsons (Eds.), *Biology of the Reptilia* (Vol. 4, pp. 101–199). London: Academic Press.

Sellers, K. C., Middleton, K. M., Davis, J. L., & Holliday, C. M. (2017). Ontogeny of bite force in a validated biomechanical model of the American alligator. *The Company of Biologists*, *220*, 2036–2046.

Sereno, P., & Larsson, H. (2009). Cretaceous crocodyliforms from the Sahara. *ZooKeys*, *28*, 1–143.

Shaker, N. A., & El-Bably, S. H. (2015). Morphological and radiological studies on the skull of the nile crocodile (*Crocodylus niloticus*). *IJAR*, *3*, 133–140.

Shiino, K. (1914). Studien zur Kenntniss des Wirbeltierkopfes. 1. Das Chondrocranium in Crocodilus mit Berücksichtigund der Gehirnnerven und Kopfgefässe. *Anatomische Hefte*, *50*, 254–381.

Soares, D. (2002). An ancient sensory organ in crocodilians. *Nature*, *417*, 241–242.

Stibbe, E. P. (1928). A comparative study of the nictitating membrane of birds and mammals. *Journal of Anatomy*, *62*, 159–176.

Tsai, H. P., & Holliday, C. M. (2011). Ontogeny of the alligator cartilago transiliens and its significance for sauropsid jaw muscle evolution. *PloS One*, *6*, e24935.

Vogel, K. S. (1992). Origins and early development of vertebrate cranial sensory neurons. In *Sensory neurons: Diversity, development, and plasticity* (pp. 171–193). New York: Oxford University Press.

Vogl, A. W., Lillie, M. A., Piscitelli, M. A., Goldbogen, J. A., Pyenson, N. D., & Shadwick, R. E. (2015). Stretchy nerves are an essential component of the extreme feeding mechanism of rorqual whales. *Current Biology*, *25*, R360–R361.

von Baczko, M. B., Taborda, J. R., & Desojo, J. B. (2018). Paleoneuroanatomy of the aetosaur *Neoaetosauroides engaeus* (Archosauria: Pseudosuchia) and its paleobiological implications among archosauriforms. *PeerJ*, *6*, e5456.

Watanabe, A., Fabre, A. C., Felice, R. N., Maisano, J. A., Müller, J., Herrel, A., & Goswami, A. (2019). Ecomorphological diversification in squamates from conserved pattern of cranial integration. *PNAS*, *116*, 14688–14697.

Wedin, B. (1953). The origin and development of the extrinsic ocular muscles in the alligator. *Journal of Morphology*, *92*, 303–335.

Wong, M. D., Spring, S., & Henkelman, R. M. (2013). Structural stabilization of tissue for embryo phenotyping using micro-CT with iodine staining. *PloS One*, *8*, e84321.

SUPPORTING INFORMATION

Additional supporting information may be found online in the Supporting Information section at the end of this article.

How to cite this article: Lessner EJ, Holliday CM. A 3D ontogenetic atlas of *Alligator mississippiensis* cranial nerves and their significance for comparative neurology of reptiles. *Anat Rec*. 2020;1–29. https://doi.org/10.1002/ar.24550